Development of a Micro-Scale Motion Capture System for Analysis of Formicidae Biomechanics

Undergraduate Research Thesis

Presented in Partial Fulfillment of the Requirements for
Graduation with Research Distinction in the Department
of Mechanical and Aerospace Engineering at
The Ohio State University

By
Sarah Farou
Undergraduate Program in Mechanical Engineering

The Ohio State University
2018

Thesis Committee:
Dr. Sandra Metzler, Advisor
Dr. Blaine Lilly

Abstract

Previous investigation has determined that ants are able to lift and support loads up to a magnitude of 1,000 times their body weight. The load path through the ant's body passes entirely through the neck, one of the thinnest structures in diameter on the ant, before it is transferred and distributed to the rest of the body. In order to gain a better understanding of the structural and material properties of the neck tissues, previous research was completed utilizing mechanical loading studies and Scanning Electron Microscopy. SEM was utilized to analyze the location of material failure in the transition region between the soft tissue and the exoskeleton. The mechanical loading study was used to determine several mechanical properties of the neck region, including ultimate failure stress and overall elastic modulus. The experimental procedure employed in the mechanical loading study involved a centripetal loading mechanism, which acted in a generally axial direction, but the method did not allow for precise measurement of either force or neck position at the time of failure. In addition, both the SEM and mechanical loading tests were performed post mortem, which did not allow for physiologically relevant positioning of the ant while lifting and carrying objects in a natural setting to be studied. The goal of this work is to explore the internal biomechanical loads of the ant neck throughout the typical physiological range of motion through in-vivo motion capture. In order to develop and validate a method of motion capture of these phenomena at a physiologically appropriate scale, two orthogonally located Go-Pro Silver 4 model cameras with macro lenses were utilized to capture relevant videos of Camponotus pennsylvanicus (Carpenter) ants, which were then processed using Tracker Video Analysis and Modeling Tool and imported into Matlab to determine the range of motion.

Dedication

This work is dedicated to my family and friends.

Acknowledgements

I would first like to express my upmost gratitude to my advisor, Dr. Sandra Metzler for her endless support, encouragement, and enthusiasm throughout my undergraduate experience. Her intelligence and professional experience has proven to be one of the most invaluable tools I have utilized in my time at The Ohio State University. She has been a wonderful mentor and role model to me and I cannot thank her enough for everything I have learned from her and for providing me with the opportunity to take on this research.

I would also like to thank Akul Kakumani for being a friend and resource during my research. Having a fellow teammate to handle the ants helped immensely with my methodology and patience of working with live ants. Thank you to Noah Einstein for introducing me to Tracker, the main image and video processing software utilized in this research, and for helping me debug my code. Thank you to George Keeney for lending me a colony of Camponotus pennsylvanicus and instructing proper care of the ants. I would like to thank Hiromi Tsuda for showing me the milling process she developed to utilize in her research and introducing me to the routine she used to take care of the ants.

Finally, I would like to thank my parents for their continuous love and support all the way from Texas. I am incredibly thankful the opportunity of attending such a prestigious university and am eternally grateful to my parents for providing me the resources to do so. Thank you for answering every frantic phone call and always knowing what to say to calm me down. Thank you to my father for immigrating to this wonderful country to pursue a better life and for being the most diligent, hardworking person I know. I will be forever grateful to you for the sacrifices you have made to provide our family with everything we have.

Table of Contents

List of Figures

List of Tables

Chapter 1. Introduction

1.1 Background

Ants have become distinguished for their ability to lift and carry loads of up to 1,000 times their own body weight. [1] Even though the load is spread throughout the torso and six legs, the neck must bear the full load prior to distribution. This is exceptional due to the neck being one of the thinnest anatomical structures on the body. As shown in the figure below, a worker weaver ant *(Oecophylla longinoda*), which weighs approximately 6 milligrams, holds a 7-gram dead baby bird at a 90 degree angle off the side of a table. To bring this phenomenon into perspective, this would be the equivalent of an 80 kg human lifting and holding a 737 airplane off a ledge. [2]

Figure 1: *Oecophylla longinoda* worker holding a dead baby bird (~1000x bodyweight). [1]

1.2 Significance of Motion Capture in Biomechanical Analysis

Applications for motion capture (mocap) can be grouped into three different groups: surveillance (monitoring), control (video games), or analysis. Most vision-based mocap systems are utilized to estimate the limb lengths and positions in human subjects through the tracking of reflective markers by infrared cameras. Various constraints, such as joint angle limits and degrees of freedom, are imposed on the body between different ratios of limb lengths to estimate a kinematic structure. [6] Kinematics is defined as the study of movement without regard to the forces that cause it and is quantified by variables such as displacements, velocities and accelerations. Along with kinematic data, kinetic data (forces that cause movement), and anthropometric data (anatomical structure) must be known in order to perform a complete biomechanical analysis. The relationship between the different types of data in relation to the calculated forces can be seen in figure 2a below, which displays the "inverse solution" to link-segment modelling. [7] Figure 2b displays the relationship between an anatomical model and link-segment model, where the joints in the leg are replaced with moments of inertia and masses located at the center of mass of each segment. Figure 2c further breaks down the link-segment model into a free-body diagram, with reaction forces and moments at each joint.

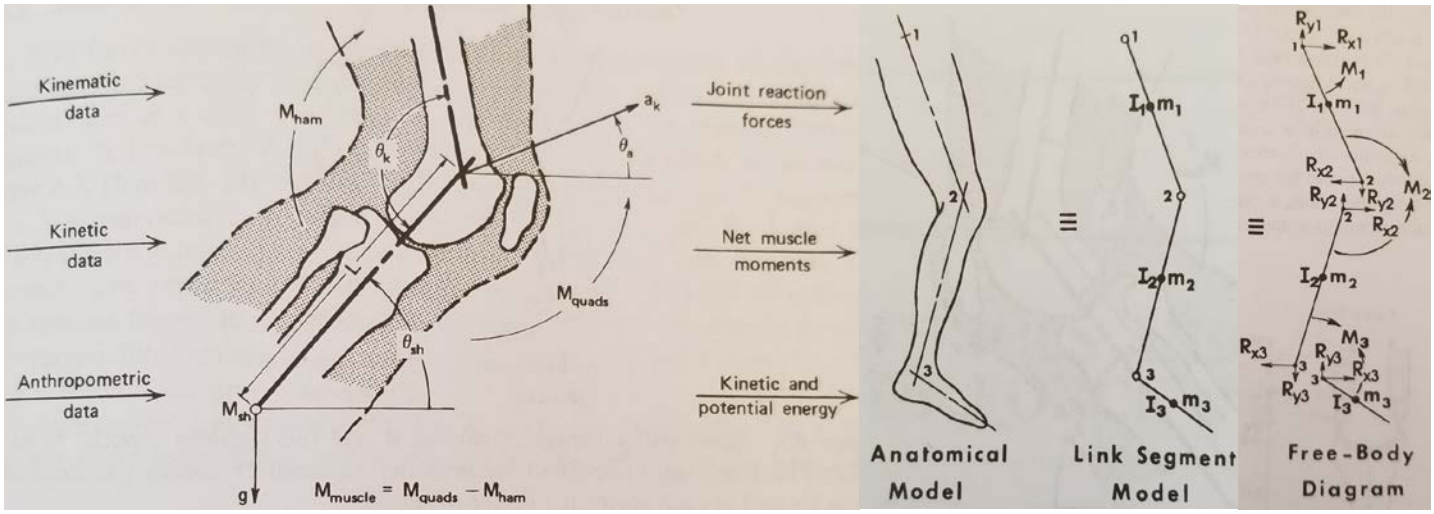

Figure 2: [A] Schematic of data to calculations relationship. [B] Relationship between anatomical and link-segment models. [C] Relationship of Free-body diagram to link-segment model. [7]

This research focuses primarily on gathering data and studying the physiological posture of ants, in order to provide information to aid in the calculation of internal force distribution in the neck joint. Similar to humans, movement constraints must be established for the ants to estimate kinematic structure. Through in-vivo motion capture, the full range of motion of the neck can be determined and utilized with the internal anatomical structures that are currently being researched. Currently, there has not been research performed to study the range of motion (ROM) of ant necks.

1.3 Previous Research

1.3.1 Ant Neck Research Exclusive to The Ohio State University

Previous research completed by masters student Vienny Nguyen focused primarily on the neck joint of the ant. Nguyen, under advisor Dr. Blaine Lilly (Associate Professor, MAE), was able to discover that the critical failure point of the neck is at the transition region between the soft membraneous tissue and the exoskeleton. Testing was done in a custom-built centrifuge with a

high speed camera to determine several mechanical properties of the neck as seen in figure 3A. Live ants were attached via the head to the platform of the centrifuge and spun at different speeds to represents different tensile loads. Elongation of the ant torso, as seen in figures 3C and 3D, was tracked through displacement of acryllic reference markers painted on the ant.

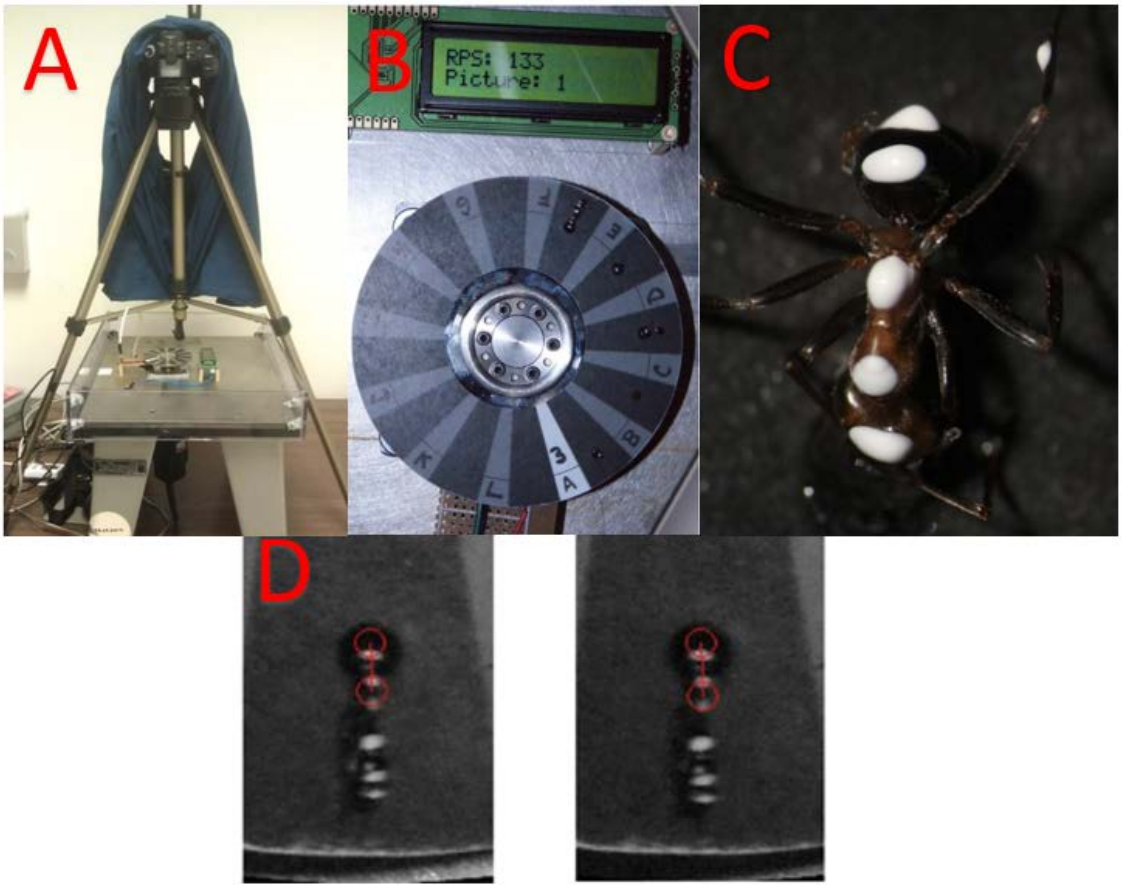

Figure 3: [A] Custom centrifuge with high-speed camera. [B] Centrifuge platform and display screen. [C] Reference markers placed in specific locations along body. [D] Tracked displacement of markers. [3]

Through the centrifuge testing, the elastic modulus of the soft tissue region was estimated to be 230 ±140 MPa, while the ultimate failure stress was estimated at 37 Mpa. [3]

In order to examine the ruptured neck in detail, Nguyen utilized Scanning Electron Microscopy.

In the detailed images below, she discovered that the interface between the soft tissue and the exoskeleton may have a stepped structure (figure 4). The geometry of the interface between the two materials could provide an explanation as to why the neck is able to bear such large loads.

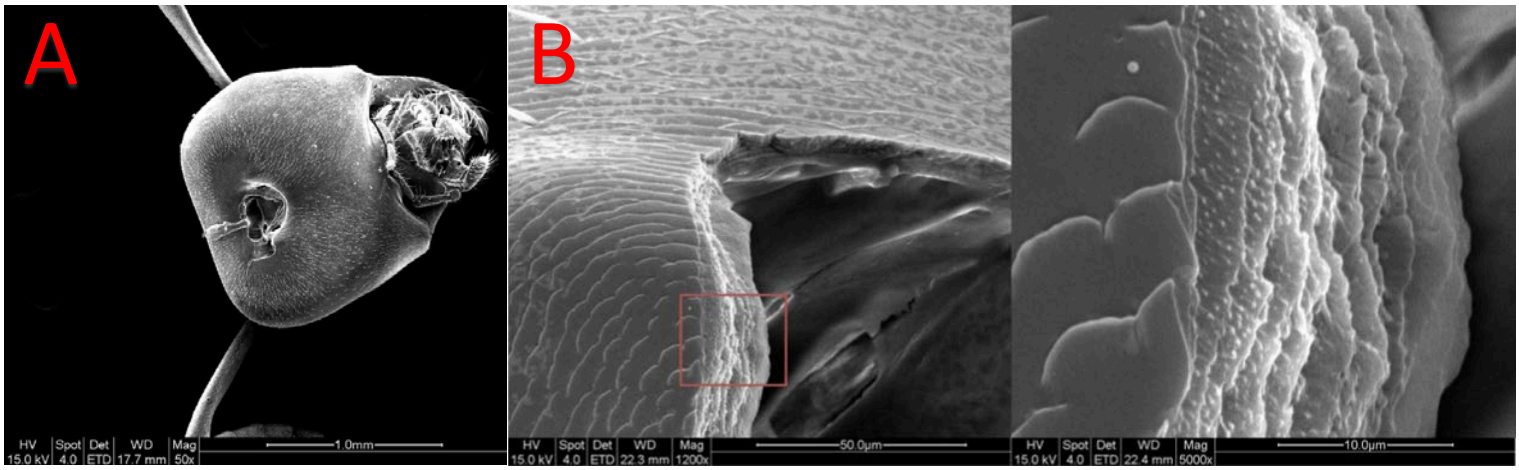

Figure 4: [A] SEM image of posterior view of a ruptured head. [B] SEM image of exoskeleton of ruptured neck. [3]

In order to gain a better understanding of the geometry of the microstructures within the ant neck, Hiromi Tsuda, under Dr. Carlos Castro (Assistant Professor, MAE) furthered Nguyen's work in SEM imaging. Tsuda concentrated primarily on the interface between the soft tissue and exoskeleton in Camponotus pennsylvanicus (carpenter ants). Her research specialized in studying how two materials with varying structural geometries and mechanical properties are able to merge and form a region that maximizes toughness. [4] Initially, specimen were prepared for SEM by manually severing the neck joint by means of blunt dissection with a scalpel or razor blade. This method did not allow for a clean cross-section to be attained, so Tsuda developed a new procedure involving casting the ants in acrylic inside an Eppendorf tube. After the deceased bodies were enclosed in resin, a very fine end mill (1/64") was used on a vertical mill in order to create a more desirable cross section, as seen below in figure 5.

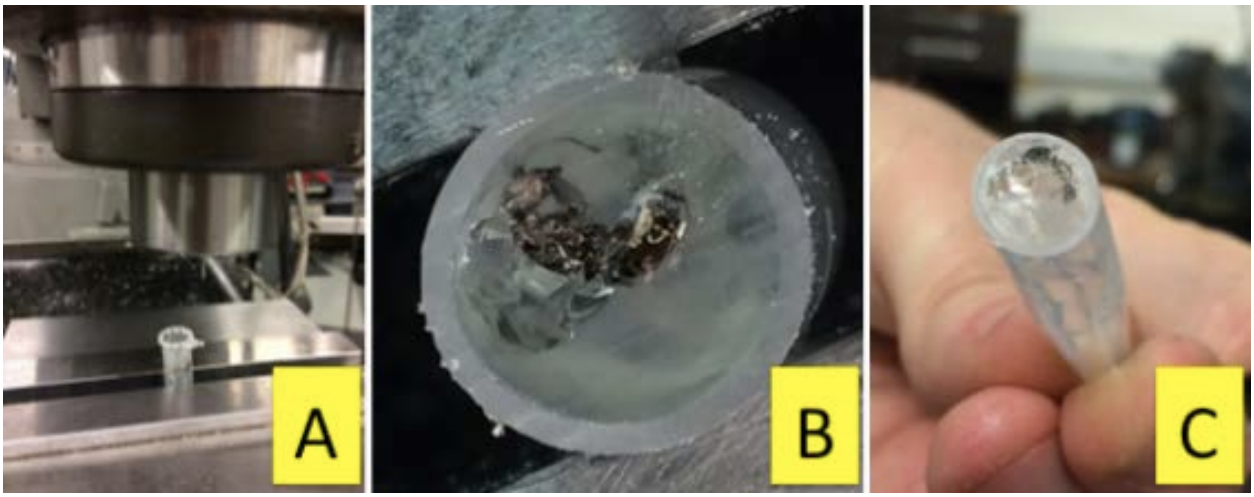

Figure 5: [A] Eppendorf tube filled with resin held in vice. [B] Final cross section after several milled passes. [C] Top view of cross section. [4]

After achieving a desired cross-section, the samples were taken to The Center for Electron Microscopy and Analysis (CEMAS) to be sputter coated and imaged with SEM. Upon imaging, Tsuda discovered fluid-filled pockets lining the soft tissue portion of the neck. These pockets are believed to aid in the elastic movements in the neck of the worker carpenter ant. [4] Shown below in figure 6, the transition region is seen, exhibiting the changes in microstructure from the elongation of the fluid-filled pockets in the soft tissue to eventually form the hard exoskeleton.

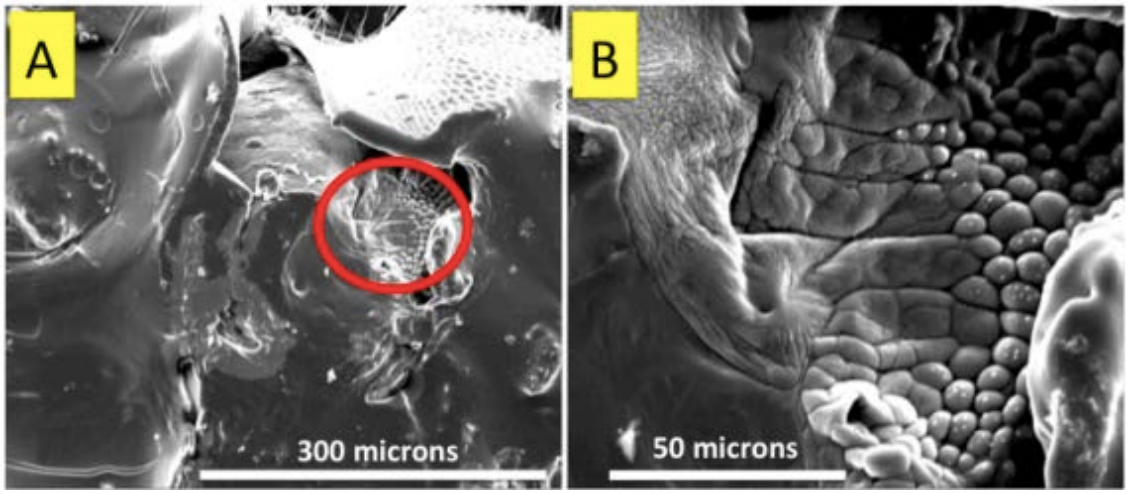

Figure 6: [A] Zoomed in portion of SEM image of transition region. [B] Close up view of transition region exhibiting changes in microstructure. [4]

The discovery of the microstructures in the transition region provides a basis that can be used to test and compare results from other species of ants in addition to Camponotus pennsylvanicus in order to understand how they are able to bear such large loads.

Following Tsuda's research, graduate student Akul Kakumani, under Dr. Sandra Metzler (Assistant Professor of Practice, MAE), designed an improved tensile tester to determine the stress and strain in the ant neck upon loading, without affecting the delicate internal structures. [5] Kakumani utilized a load cell with a range of 0.1 to 5N to test not only the accuracy of value obtained by Nguyen (0.33 N), but a significantly wider range of values. To track displacement, a highly sensitive displacement sensor was used within the range of micrometers. As seen below in figure 7, when the neck ruptures and pulls apart, the body is still held to the head by a thin membrane.

Figure 7: Ruptured neck held together by membrane. [5]

Through testing, Kakumani found the average value of the rupture load to be 0.21N, verifying Nguyen's previous value.

1.3.2 Capture and Synthesis of Insect Motion by Gibson, Oziem, Dalton, and Campbell [8]

In the U.K., scientists conducted motion capture on tarantulas and European wood ants to develop computer-generated models of motion synthesis. Their process involved combining autoregressive processing with segment copying to dynamic programming that reduces user input. Three high-speed cameras placed orthogonally to each other with a speed of 150 fps were used to film the ants. Instead of placing markers on the ants, a 22-point static calibration system was utilized. Even though a significant amount of footage was collected, only short clips were utilized for motion extraction. After running the data through several algorithms, the generated segments were analyzed against the original segments. The proposed system successfully captured motion synthesis of the insects, while reducing user input.

While the results were successful in tracking the general patterns of movement in ants and tarantulas, since markers were not placed on the insects, this study does not capture the posture of the ants or produce data that would aid in biomechanical analysis.

1.3.3 Compter-Assisted 3D Kinematic Analysis of All Leg Joints in Walking Insects [9]

An open-source software was developed in Python to simultaneously analyze points on each leg of an insect and derive 3D kinematic data. Experimentation involved the use of adult female cockroaches, Blaberus discoidalis. The cockroaches were tethered with a small piece of plastic to enable slight dorsal-ventral flexion, post anesthetization via ice, and marked with white paint on their leg joints, as seen below in figure 8. Two high speed cameras were positioned beneath the glass to capture multiple ventral views of the insect walking. Video lengths of 8 seconds with camera speeds of 50 fps were recorded to obtain 4096 frames for analysis. The

positions of the cameras were calibrated utilizing an open-source software and had a triangulation error of 0.3mm. Prior to tracking, a Gaussian filter was used to increase the signal-to-noise ratio.

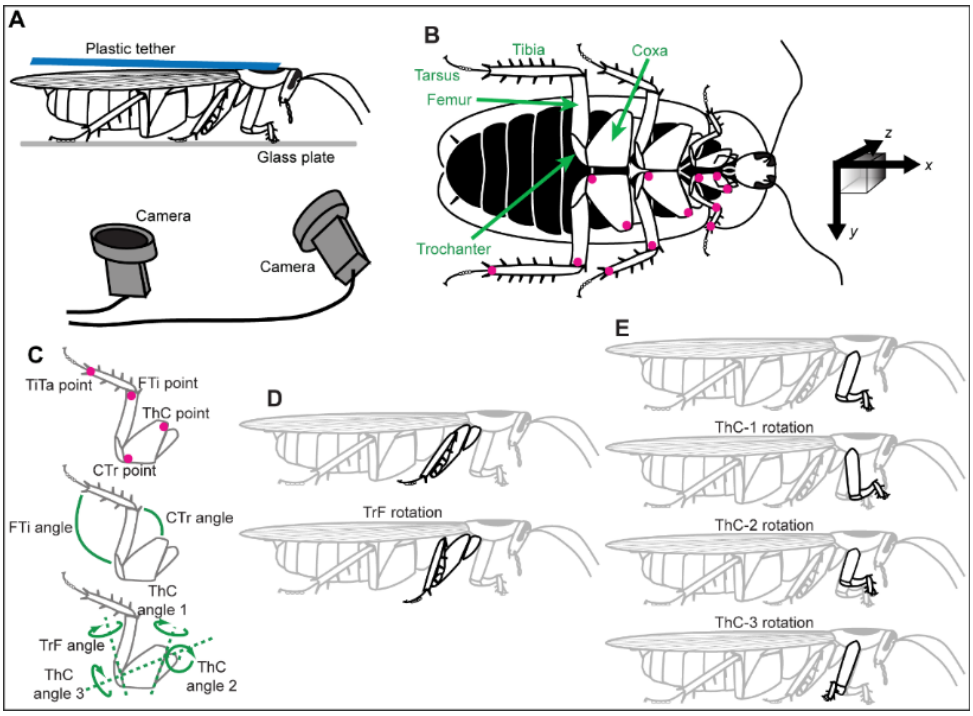

Figure 8: [A] Schematic of cockroach with plastic tether on glass plate. [B] Ventral view of roach. [C] Marked points on leg joints. [D] Joint reduction of trochanter-femur to lower foot. [E] Three-degree rotation of thorax-coxa. [9]

The initial position of each joint was defined by the user, followed by automatic tracking from the program to estimate positions of each joint. Some frames required manual editing to fix mismatches, but the overall program accuracy was within 95-97% of locating points. The process was able to produce results with a similar accuracy to manual digitization. Figure 9 includes a bar graph of the mean and standard deviation of the 3D distance from the manually derived points to the points obtained from the software over the span of 4096 frames.

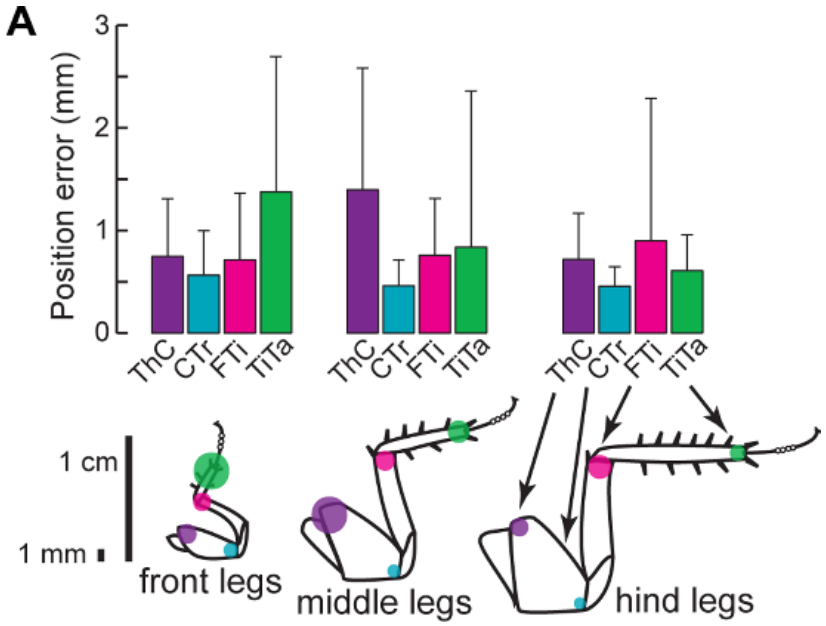

Figure 9: Bar graph of mean and standard deviation of each leg. [9]

This study produced exceptional overall results, with and average tracking error, less than 1mm. Even though the strides of the cockroach were able to be accurately tracked, without the knowledge of muscular structure and joint constraints, internal forces are unable to be analyzed. In addition, due to the difficulties in collecting large enough kinematic datasets, a majority of parameters of insect behavior and motion are unanalyzed. Since the internal structure of the ant neck has been previously researched in detail, studying the posture of the ant while performing various movements will aid in the analyses of internal force distribution in the neck.

1.4 Focus of Thesis

This independent research, under Dr. Sandra Metzler (Assistant Professor of Practice, MAE), is a continuation of research on the ant neck joint exclusive to The Ohio State University, specifically investigating the biomechanics of the ant neck through in-vivo micro-

scale motion capture. The use of motion capture through two orthogonally mounted Go Pro Silver 4 cameras with macro lenses allows for the observation of physiological positioning of the ant. Once the natural range of motion is discovered through image and video processing software, the internal biomechanical loads on the neck can be investigated. Unlike previous research on insect motion capture, this research focuses on studying the posture of the ant through markers on the ant itself, rather than tracking overall patterns of migration.

1.5 Significance of Research

The goal of this work is to develop a micro-scale, affordable motion capture system to observe the ants in a natural setting. In addition to this specific research, the motion capture system can be utilized to perform research on ideally any micro-scale object, similar to the size of an ant. Understanding the range of motion of the neck joint can assist in understanding how the internal forces are distributed in the neck. This will allow for exploration of the relationship between tissue strength and external loads. From an engineering perspective, with an understanding of the limitations of the range of the neck joint, it may be possible to create structures or materials that are able to bear loads of similar magnitudes. This could eventually aid in the development of prosthetics with exceptional load bearing capabilities.

1.6 Overview of Thesis

This thesis contains four chapters. The first chapter contains the introduction and background information from previous research, along with research previously completed

exclusively at The Ohio State University. Chapter 2 contains the materials and methodology of the research, including the setup, calibration, and step-by-step procedure used during filming and video post-processing. This chapter also includes development of the designed prototype in which the ants were filmed, along with protocol for care of the ants. Chapter 3 provides an in-depth analysis of the results obtained from the collected data. Chapter 4, the conclusion, will summarize the work and provide limitations and guidance for future research.

Chapter 2: Materials and Methods

2.1 Ants

2.1.1 Obtainment of Colony

A colony of Camponotus pennsylvanicus (Carpenter ants) was obtained in the fall of 2015 from the insectary located in the Biological Sciences Greenhouse Facility. Since Allegheny Mound Ants, *Formica exsectoides*, were unavailable, this research was conducted with carpenter ants instead. George Keeney, insectary manager, provided approximately 80-100 ants that ranged from 5mm to 15mm in size. The colony included worker ants and a queen to produce brood (offspring). The ants were transported and stored in a plastic container that had a coating of Fluon painted around the top inch to prevent the ants from escaping when the lid was removed. The initial colony provided survived two years with proper care. A new colony of C. pennsylvanicus ants, similar in size, was obtained in January, 2018 to complete research. The new colony received the same care and was passed on to fellow research student, Ryan Wilber, to continue research on the ants.

2.1.2 Care of Colony

Figure 10: Overhead view of colony setup.

The colony was kept in a room with minimal sunlight exposure at a temperature range of 65 to 75 degrees Fahrenheit. The container that the ants lived in contained 5 glass test tubes that were filled 1/3 of the way with water, tin foil that covered the opening of the test tubes, a sugar cube, and a small foil tray for food. A cotton ball was stuffed inside the tubes to keep the water in and allow for a high level of humidity. The tubes were refilled with water about once a month, when the original water had evaporated, and the cotton balls were replaced. A sheet of tin foil also covered the test tubes to prevent light exposure. The tubes were kept in place by a layer of clay stuck to the bottom of the plastic container. The ants were fed a diet of Bhatkar's agar, three times per week, which consisted of: honey, egg, agar, salt and water, along with dried meal worms on occasion. Two containers of agar were provided from the insectary, which were kept frozen to prevent mold growth. When the provided agar was depleted, the following recipe from "Journey to the Ants" was followed. [12]

1 egg
62 ml honey
1 gm vitamins

1 gm minerals and salts
5 gm agar
500 ml water

Dissolve the agar in 250 ml boiling water. Let it cool. With an egg beater mix 250 ml water, honey, vitamins, minerals, and the egg until smooth. Add to this mixture, stirring constantly, the agar solution. Pour into petri dishes (0.5-1 cm deep) to set. Store in the refrigerator. The recipe fills four 15-cm diameter petri dishes, and is jellylike in consistency.

The batch yielded four containers of agar that were stored in the freezer for maximum shelf life.

2.1.3 Marking Procedure

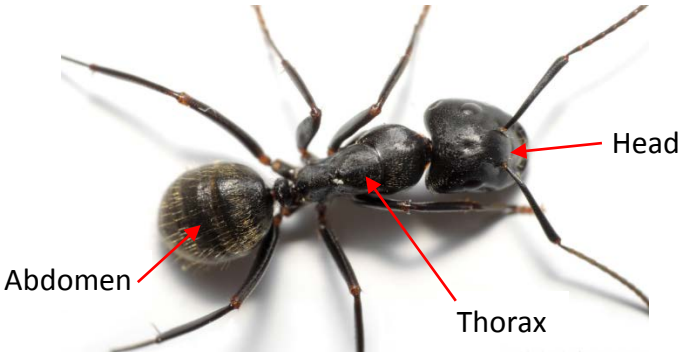

Figure 11: Anatomy of an ant. [17]

In order to accurately track posture, markers were applied to the head, thorax, and abdomen with acrylic paint. Acrylic paint was chosen due to its non-toxic nature and ability to easily be applied to and removed from the ants. Multiple tools were used to create markings on the ants including nail art tools with spherical balls, pipettes, paint brushes, cotton swabs, and toothpicks. The nail art tools and pipettes were able to produce circular markings, but the diameters on average were larger than desired (>1mm). The paint brush and cotton swabs did not produce sufficient

markings and were eliminated as options. It was found that toothpicks were able to repeatedly produce markings with diameters of 1mm and under. Since the two cameras were placed orthogonal to each other on the top and side of the testing environment, the paint needed to be applied in a spherical shape in order to allow the side camera to view the markings. Shown below in figure 11 are images of different ants that were marked with toothpicks. Initially, ants were marked on the head, thorax, and abdomen with white acrylic paint. However, when the videos were imported into Tracker, there was not a clear way to distinguish each marker from the others. To differentiate the markers, multiple combinations of blue, red, green, and yellow paint were used on each ant. The table below lists the ants in order that they were filmed, designated by their unique marker combination. Prior to marking with paint, the desired ant, in a small plastic container, was placed in a freezer with temperature of 0 degrees Fahrenheit for anesthetization purposes. Ants were only stored in the freezer for 3 to 5 minutes to prevent death from occurring. After the ant was marked with paint, the ant was placed back in the small plastic container to allow the paint to dry without smudging. Once the paint was dry, the ant was placed in a separate plastic container that temporarily contained all of the marked ants. Ants were extracted from colony container and transported via cotton swab to minimize the possibility of injury.

Figure 12: Different color combinations of markers.

	Head Marker	Thorax Marker	Abdomen Marker
Ant 0	White	White	White
Ant 1	Green	Yellow	Red
Ant 2	Blue	Yellow	Red
Ant 3	Red	Yellow	Blue
Ant 4	Yellow	Red	Blue
Ant 5	Blue	Green	Red

Table 1: Combinations of Color Makers

Limitations to the marking process included the ability to only mark one ant at a time, due to the anesthetization process in the freezer and the need to manually blow on the paint to speed up the drying process. The ant was held on a cotton swab to prevent smearing of the acrylic paint while it dried. Testing was performed the same day as the marking procedure due to the ants behavior of rubbing the markers off themselves and the other ants.

2.2 Experimental Equipment and Set-Up

2.2.1 Camera Selection

Since this research was conducted on a micro-scale level, the use of a high-resolution, high-speed camera was necessary. Highly accurate motion capture camera systems capable of focusing on objects as small as insects cost up to tens of thousands of dollars and do not contain reflective markers small enough to place on an ants body. The goal of this research is to created a motion capture system that is accurate and can be easily recreated by any user, i.e., the whole system needs to be relatively inexpensive. The Go Pro Hero Silver 4 was selected due its relatively inexpensive cost (<$400) and versatility. Shown in figure 12 below, the camera is capable of recording resolutions from 720 to 4K, with fps that range from 12.5 to 240. A key feature of the camera that aided in the calibration of the camera with the filming environment was availability of the multiple field of view (FOV) options.

HERO4 Silver

Video Resolution	Frames Per Second (fps) NTSC/PAL	Field of View (FOV)	Screen Resolution
4K	15, 12.5	Ultra Wide	3840x2160
2.7K	30, 25, 24	Ultra Wide, Medium, Linear	2704x1520
1440p	48, 30, 25, 24	Ultra Wide	1920x1440
1080p	60, 50, 48, 30, 24, 24	Ultra Wide, Medium, Linear, Narrow	1920x1080
1080p SuperView	60, 50, 48, 30, 25, 24	Ultra Wide	1920x1080
960p	100, 60, 50	Ultra Wide	1280x960
720p	120, 60, 50, 30, 25	Ultra Wide, Medium, Narrow	1280x720
720p Superview	100, 60, 50	Ultra Wide	1280x720
WVGA	240	Ultra Wide	848x480

Figure 13: Chart of Go Pro Hero 4 Silver Settings. [18]

2.2.2 Macro Lens Selection

Depth of field (DOF) is defined as "the zone of acceptable sharpness within a photo that will appear in focus." [14] The depth of field is controlled by the aperture (f-stop) of the camera, the distance of the subject from the camera, and the focal length of the lens. The aperture refers to the diameter in which light enters the camera, while the focal length of the camera is the optical distance from the convergence point of the image to the digital sensor. [15] In simpler terms, the focal length of the camera determines the size of the image produced, along with the field of view (FOV) (amount of scene captured). Since the f-stop of the GoPro (f/2.8) and the distance of the subject from the camera are not adjustable, the depth of field was only able to be manipulated by the addition of a macro lens.

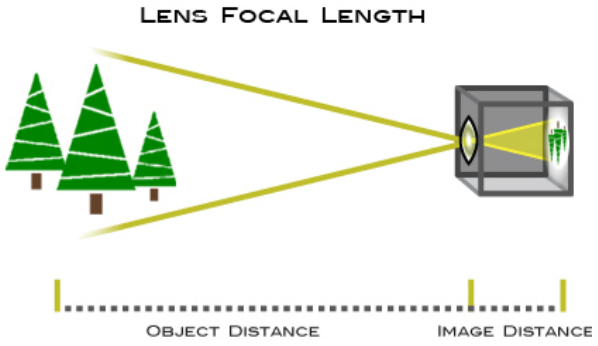

Figure 14: Focal length diagram. [15]

Initially, testing was executed with just the GoPro, but the videos were significantly blurry, indicating the need for a macro lens. Two lenses were evaluated, the Polar Pro 3.8x magnification macro lens, and the Neewer 12.5 magnification macro lens. As seen in figure 13, the Polar Pro macro lens attaches to the outside of the diving house, resulting in the mandatory use of the housing during recording. Without the housing, the distance from the bottom of the camera to the center of the lens is 1.125 inches, which increases to 2.5 inches when the housing case and stand are added. Since the center of the camera lens should be level to the surface, the use of the Polar Pro lens

would require the camera to sit on a surface lower than the environment being filmed. In addition, the diameter of the Polar Pro lens was significantly larger than the Neewer lens and would require a design change to the testing environment windows, that has potential to allow the escape of ants during filming. During a calibration test executed by placing a dead ant on a grid with 0.5" incremental markers, the Polar Pro lens was able to produce better resolution than the Go Pro alone, but was only able to focus on objects approximately 3-8 inches away.

Figure 15: Polar Pro 3.8x Magnification Macro Lens for Go Pro Hero 4. [10]

The Neewer macro lens, compatible with the Go Pro Hero 3 & 4 models, included an adapter ring that fit around the lens of the go Pro without the housing, as seen in figure 14. The diameter of the lens did not affect the distance from the ground to the center of the lens, which made it significantly more convenient to modify the design to the testing environment. In addition to the magnification increase to 12.5, through the calibration testing, the lens was able to focus on objects between 15 and 55 mm, which is a more relevant focal range for filming ants. This lens was able to produce significantly clearer images than the Polar Pro lens and was overall more favorable in design.

Figure 16: Neewer 12.5 magnification macro lens for Go Pro Hero 3, 4. [11]

2.3 Testing Environment Design Development

2.3.1 Initial Prototype (1.1)

Since ants move at high speeds and are able to climb on virtually any surface, a testing environment from which the ants are unable to escape was a necessity for this research. The first prototype, shown in figure 11, had side lengths of 4.98”, keeping the total volume under 125 in^3, which was the size limit of the 3D printer utilized. If the environment had needed to increase in size, a different 3D printer would have been utilized. However, after testing prototype 1.2 (same overall dimensions), the size was actually found to be too large, indicating the 3D printer was sufficient for printing. The walls had a thickness of 0.39” and a 1” square window (cutout) for the Go Pro lens to fit inside. The window was located 0.5” off the ground to allow the GoPro to sit level with the environment. Since there was no top to the enclosure, a layer of Fluon was applied around the top inch of the walls to prevent the ants from escaping.

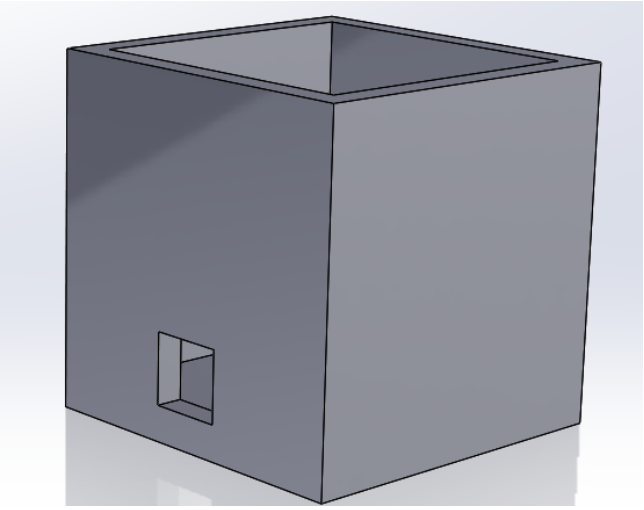

Figure 17: Ant Environment Prototype 1.1.

Testing in the environment was limited to a single camera view, and was performed prior to the addition of a macro lens. Due to these limitations, the prototype was revised to include spots for two orthogonal cameras, and to fit the diameters of the Neewer macro lenses.

2.3.2 Prototype 1.2

The dimensions of the second prototype remained the same, with the exceptions of the thickness of the front wall increasing to 0.75” to allow for the elongation of the distance of the lens to the Go Pro body caused by the macro lens adapter. The prototype, as seen in figure 16, was designed for the macro lens of the side camera to sit flush with the inner wall of the environment. Since the diameter of the macro lens measured 1.5”, the windows were designed with a diameter of 1.625” to allow for a 1/8” clearance. The top of the environment included a 1” deep, removable structure to hold one of the GoPros 3” above the ground. The holder fit into slots on the main environment was designed to have enough of a clearance around the body of the GoPro to allow

the user to press the record button located on the top right corner. To allow for the lens to be centered over the environment, the left arm of the holder was set to 1.2”, while the right arm was 0.4” long.

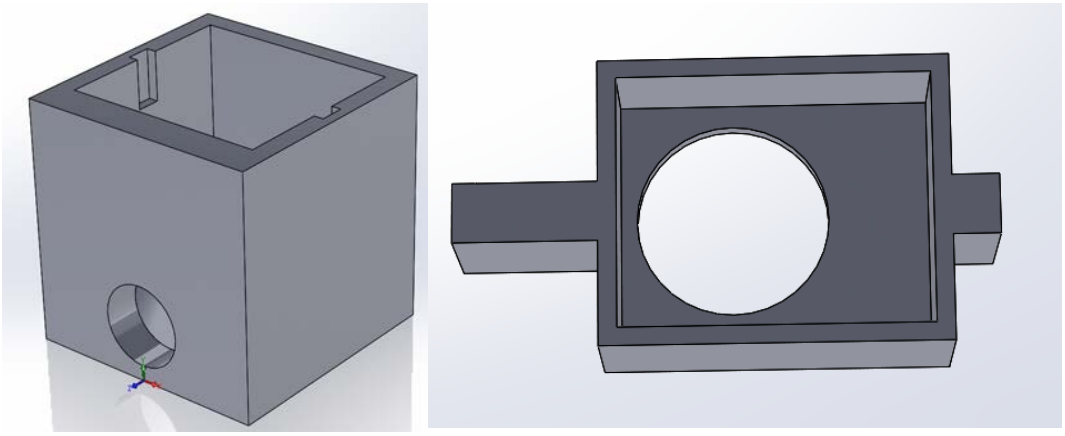

Figure 18: Ant Environment 1.2.

Since the distance from the ground to the center of the Go Pro lens was not accounted for in the initial design, and the camera was not level with the ants being filmed inside. In addition, this environment proved to be too large for filming, as the range that the macro lenses were able to focus clearly were significantly smaller than the size of the environment. Through a calibration test that is discussed later in this paper, it was discovered that the macro lens was only able to focus from depths of 15-55 mm, which resulted in the ants being out of focus a majority of the time during filming.

2.3.3 Prototype 1.3

Due to the limited range of focus of the macro lens, prototype 1.2 was scaled down to allow for a better range of focus while filming. The thickness of the front wall remained 0.75”, but the inner wall-wall width decreased to 3”. The depth of the environment was reduced to 2.82” to allow for the lens to be centered in the environment and to allow for a clearance between the holder and

front and back walls of the environment. Due to the location of the GoPro lens relative to the body, lens was not centered width-wise in the environment. The offset did not cause significant difficulty while filming.

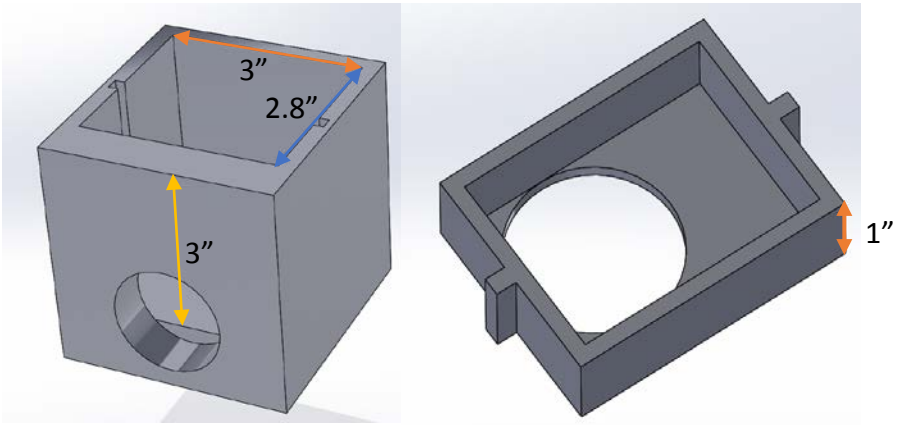

Figure 19: Final Prototype (1.3).

This prototype allowed for successful focus of the ants while filming, with the exception of the ants attempting to climb up the walls to escape, or being located outside of the radius of focus of the lens (discussed in the next section).

2.4 Experimental Set-Up and Calibration

2.4.1 Go Pro Calibration

In order to determine the best combination of resolution and speed for the GoPros while filming, a calibration test was set up. The test consisted of utilizing a grid of 5x5 mm squares along the bottom and back interior wall of prototype 1.2 to determine the focus range of the macro lens. Prior to testing, it was determined that the ideal combination of GoPro settings with the macro lens, in order to minimize file size, was 1080p with a wide FOV and a speed of 30 fps. These settings resulted in exceptional video resolution with enough frames to track the movement via software. Once these settings were established, testing was performed by placing a dead ant in the

center of each grid marking, as seen in figure 18A, to find the DOF and FOV of the macro lens. Without the macro lens, the GoPro has an f-number of 2.8 and a focal length of 17.2 mm on the wide FOV setting. [##] As previously stated, the GoPro does not have an adjustable DOF, so the Neewer macro lens was added to manipulate the DOF and FOV. Since the focal length of the lens was not provided by the manufacturer, both the DOF and FOV were determined by the calibration test. The test utilized a qualitative visual check, confirming whether the ant was in clear focus or was less focused/blurry. The DOF ranged from a distance of 15 – 65 mm from the lens (50mm), while the FOV had a range from 30 mm from the inner left wall of the environment to 75 mm from the inner left wall (45 mm). The field of focus on the grid (combination of DOF & FOV) is highlighted in pink in figures 19B &19C. For the distance of the lens of the top camera to the floor of the environment, the average value of the DOF range was taken (40 mm) as the value for the height for prototype 1.3.

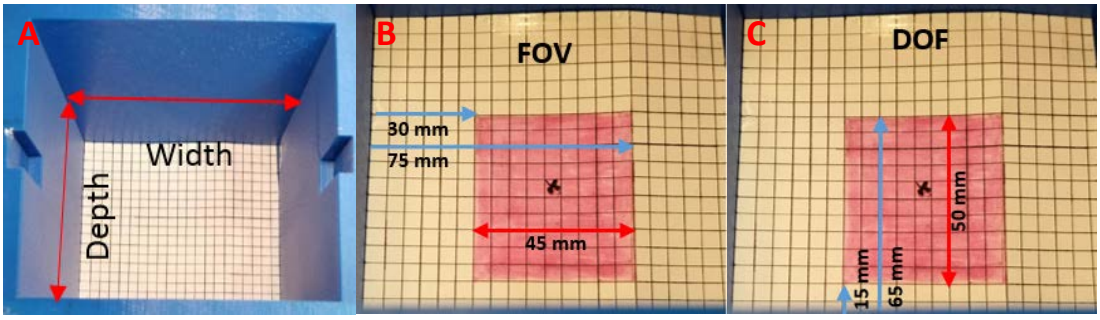

Figure 20: [A] View of Calibration Grid in Prototype 1.2. [B] Highlighted Field of View. [C] Highlighted Depth of Field.

After scaling down prototype 1.3 to the proper dimensions, another calibration test was performed with the same process to confirm the previously determined DOF and FOV. The results were consistent with the test of the larger environment. After utilizing Tracker video processing software for post processing, it was determined that a calibration tool was needed in the environment to create a common origin between both cameras and to properly scale the coordinates

that were output. The tool below was developed in SolidWorks and 3D printed. It is orthogonal on all three sides and has side lengths of 10 mm.

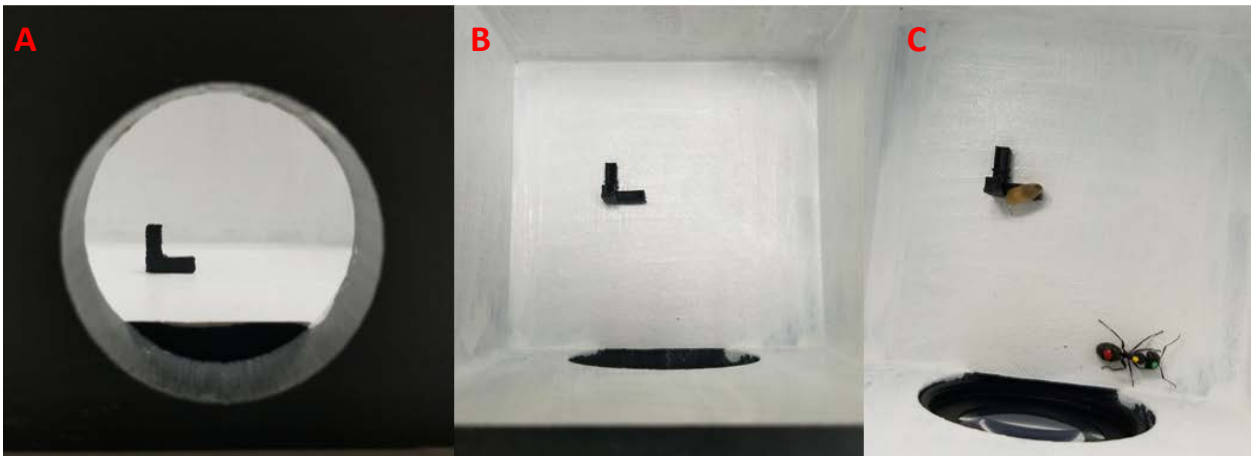

Figure 21: [A] Side View of Calibration tool. [B] Top View of calibration tool. [C] Marked ant in environment with brood.

The calibration tool was placed 35mm from the front wall and 20mm from the left wall and was used as an axis reference for both cameras during data processing in Tracker.

2.4.2 Experimental Set-Up and Procedure

Once the calibration for the Go Pros with the macro lenses was completed, the experimental set-up and procedure were formulated. Figure 20 shows the experimental setup, consisting of prototype 1.3, two orthogonally mounted GoPro cameras with macro lenses, and a large LED lamp to provide light. The lamp was positioned in several locations to find the best orientation for lighting of both the top and side cameras. It was found that positioning the lamp an eighth of an inch above the gap between the front interior wall and top camera holder produced the best combination of lighting for both cameras.

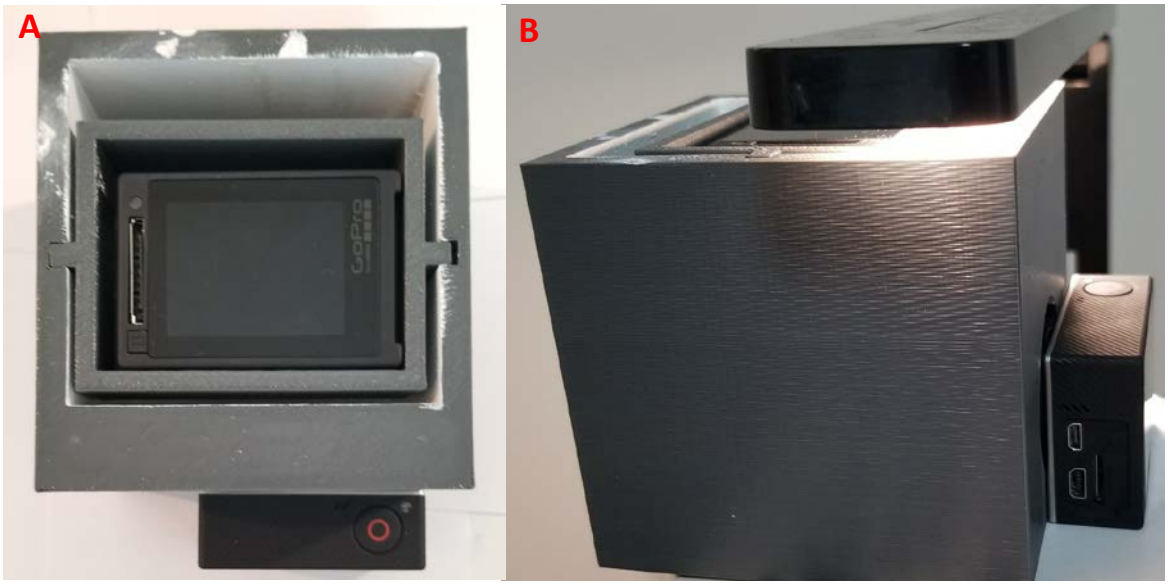

Figure 22: [A] Top view of orthogonal cameras without lamp. [B] View of complete setup.

Once the set-up and calibration were complete, the following protocol for testing was developed. A marked ant was extracted and placed inside the testing environment with a single brood (larvae). The brood was placed in the environment as incentive to lift and carry, as the worker ants are very protective over their unborn larvae. The two GoPro cameras were set to the appropriate settings and the record buttons were pushed simultaneously on both cameras. Each ant was filmed anywhere from 5 minutes to two hours, depending on the magnitude of its movement inside the environment and battery capacity of the cameras. Once the ant was filmed for an appropriate amount of time (ant was positioned in front of side camera for a few seconds), the cameras were stopped and the ant was extracted and placed back into the appropriate container. Post-filming, the videos were trimmed and imported into a video processing software (Tracker) to track the markers.

2.4.3 Video Processing

An open-source software called Tracker was utilized for tracking the markers on the ant relative to the calibration tool. Since the cameras were orthogonal, they shared a common x-axis, which was used to evaluate the error of measurements. The following procedure was utilized in Tracker to standardize the tracking of markers. First, the coordinate axis was established on the left edge of the calibration tool for both the side and top view videos. Then, the calibration stick in the software was set to the length of the calibration tool in the environment (10mm) to properly scale the coordinates. This setup can be seen below in figure 22. Since Tracker is set in real world coordinates (unitless), the software is very versatile in that it can be set to any scale without a conversion factor. Once the coordinate axis and calibration stick are set, a set length of frames to be analyzed it set. Due to the nature of movement and speed of the ants, clips with 30-40 frames in duration were used. Even though this is between one and two seconds of actual time, this number of frames provides a sufficient number to analyze whether the x coordinates between both cameras are within an appropriate range of each other. Each marker on the ant is defined as a point mass and tracked relative to the coordinate axis for the desired amount of frames. The markers are tracked based on the template defined when the point mass is chosen. The autotracker feature was used to automatically match points to the defined template. This feature does not work well when the ant turns around in the video and the marker is visually obstructed in the side camera view. When this occurs, or if the autotracker identifies the incorrect point, the software includes an override in which the user can manually set the tracking point. As seen below in figure 21, Tracker outputs data from the two coordinate axes vs. time, in addition to a graph of x-coordinates vs. time.

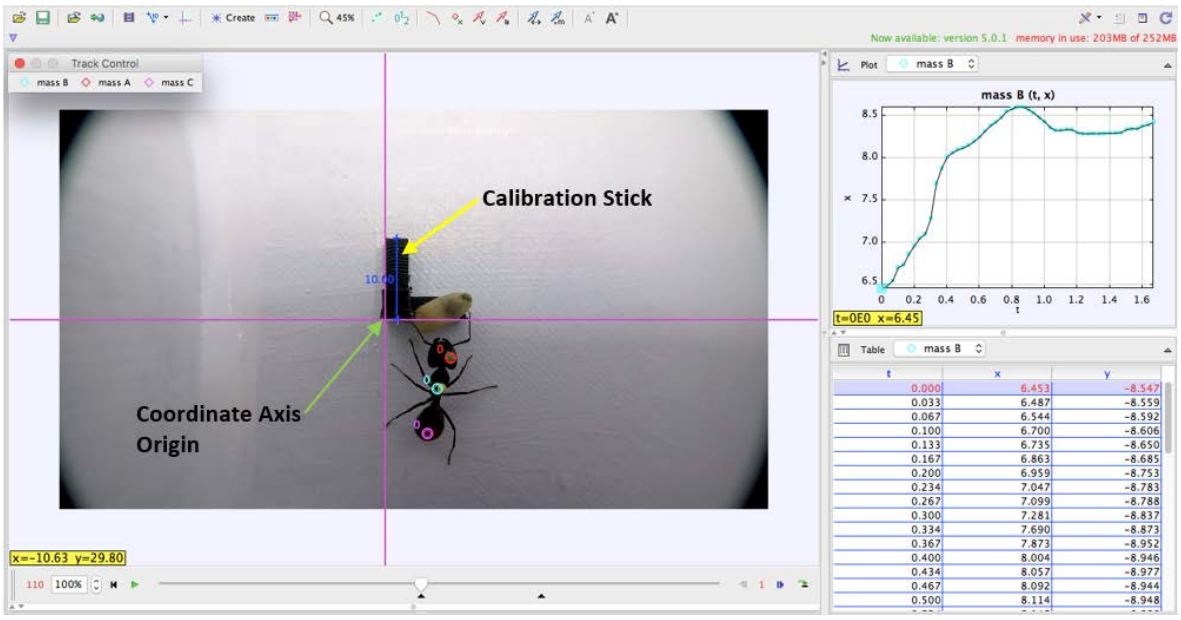

Figure 23: View of top camera video in Tracker with calibration stick, coordinate axis origin, and set point masses.

Data from tracker was imported into Excel to compare the error of the x coordinates from the front and side videos. Graphs were created for x position vs. time, along with error between the two camera views. Once the data was processed in excel, it was imported into Matlab to determine the 2D and 3D angles of the neck. The code was developed to convert the coordinates into vectors, then take their dot products to find the equivalent angles. Once the angles were graphed, the minimum and maximum values for each ant were extracted to analyze the range of motion.

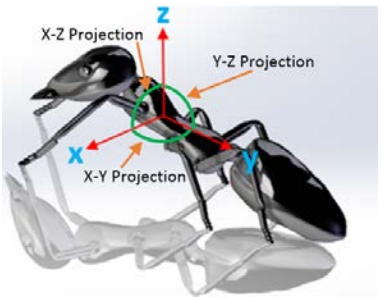

Figure 24: 2D Ant Angles. [16]

Chapter 3: Results

3.1 Results from Tracker

As previously stated, preliminary testing was completed before the testing procedure was developed. Ant 0, with three white markers, was filmed in the environment prior to the addition of the calibration tool. Since the average marker size of the ants was between 0.5 and 1 millimeter, the goal was to have a position error of less than 1 millimeter between the cameras. As seen in figure 22 below, the difference between the x coordinates for the head marker on Ant 0 is significantly over 1 millimeter during the first 15 frames (0.5 second). This is due to several factors: the use of the brood placed in the environment for the coordinate axis origin between the two cameras, the rough estimate of the length of the brood to scale the coordinate system, and the turning motion of the ant away from the camera resulting in the loss of vision of the marker. The overall average error for the head marker was 1.04 millimeters, while the thorax and markers increased to 1.13 and 1.67 millimeters. This was due to the loss of vision of the markers during the video as the ant turned away from the camera.

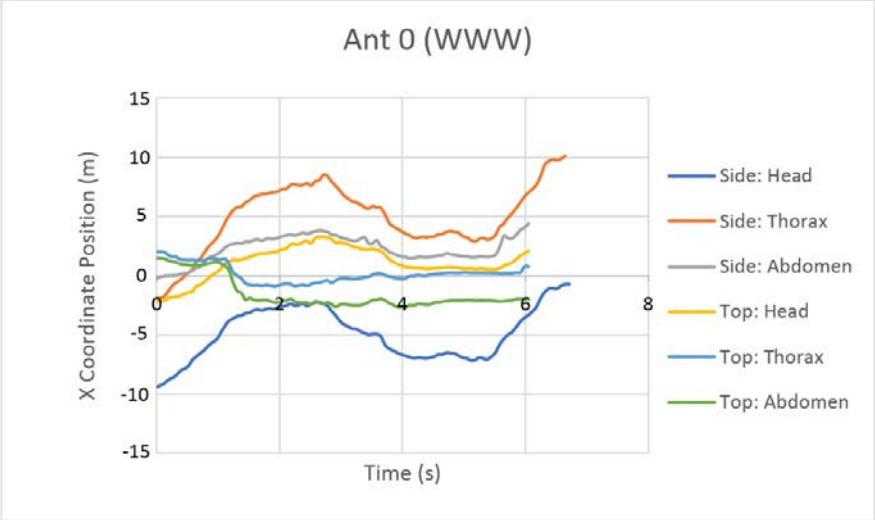

Figure 25: X-Coordinate Position Vs. Time for Ant 0.

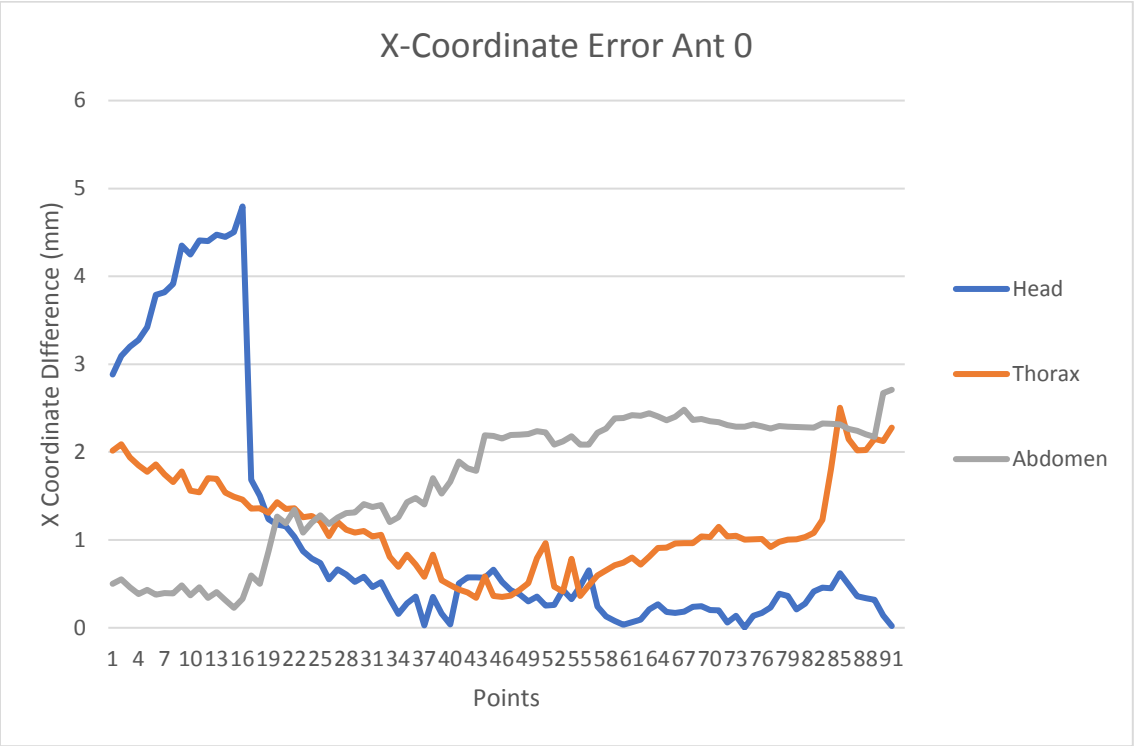

Figure 26: X-Coordinate Error Vs. Frame for Ant 0.

Once the calibration tool was introduced (Ants 1-5), the error between the x coordinates decreased to values below one millimeter, which was the desired outcome. As seen in table 2 below, the abdomen tends to yield the highest error out of the three markers due to a couple of factors. The markers on the abdomen typically were at the upper diameter size (~1mm), while the head and thorax markers were usually between 0.5 and 0.75 mm. In addition, the abdomen markers were most difficult to track due to the nature of movement of the ant. In most of the videos, the ants are travelling at quick speeds and turning away from the camera, which requires the use manual override of autotracker to select the points by hand. The abdomen marker had the highest occurrence of manual point selection.

	Head	Thorax	Abdomen
Ant 0	1.04 mm	1.13 mm	1.67 mm
Ant 1	0.37 mm	0.14 mm	0.55 mm
Ant 2	0.52 mm	0.41 mm	0.79 mm
Ant 3	0.09 mm	0.44 mm	0.29 mm
Ant 4	0.29 mm	0.23 mm	0.21 mm
Ant 5	0.55 mm	0.49 mm	0.88 mm

Table 2: Average Error for X-Coordinates Per Marker

The graphs for ants 1 through 5 can be seen in the appendix.

3.2 Matlab Results

Once the coordinates from the excel file were uploaded into Matlab, they were converted into two vectors between the head and thorax and thorax and abdomen. Using these vectors in 3D space, the angle between those vectors were obtained using the dot product shown below.

$$\theta = \text{acos}\left(\frac{vector_1 \cdot vector_2}{||vector_1|| * ||vector_2||}\right)$$

where: $vector_1 = < x_1 - x_2,\ y_1 - y_2,\ z_1 - z_2 >$

$vector_2 = < x_2 - x_3,\ y_2 - y_3,\ z_2 - z_3 >$

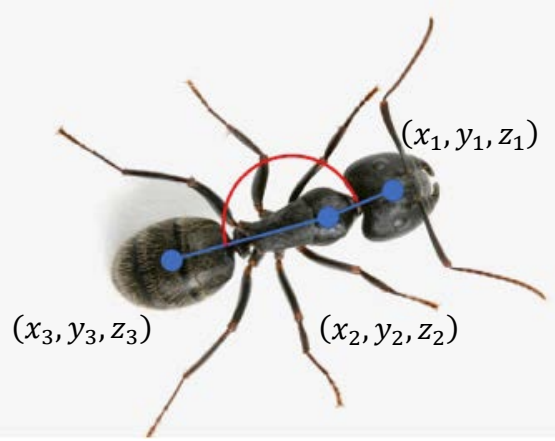

Figure 27: 3D Angle Created From Marker Vectors. [17]

The minimum and maximum angles were extracted to represent the range of motion of the head relative to the thorax for each ant in the time span of the video. Since the videos contained only enough frames to represent 1-2 seconds of motion, the range of the angles does not represent the maximum range of motion of each ant, but can be used to provide a basis for future research. Table 3 contains the minimum and maximum angle values obtained from each of the videos.

	Minimum Angle (Degrees)	Maximum Angle (Degrees)	Range (Degrees)
Ant 0	5.31	38.37	33.06
Ant 1	14.41	24.71	10.3
Ant 2	20.57	30.55	9.98
Ant 3	0.00	0.05	0.05
Ant 4	11.21	26.01	14.8
Ant 5	2.87	17.20	14.33

Table 3: Range of Motion of Ants

For the ants that were filmed with the properly calibrated environment (1-5), the neck exhibited a range of motion between 10 and 15 degrees, with the exception of ant 3. Since there was not a significant change in the posture (markers did not have much displacement relative to each other) of ant 3 during movement, this would be useful in a static biomechanical analysis of the internal load distribution. In order to perform a static biomechanical analysis of the internal load distribution, there would have to be a known external load applied to the ant neck, along with knowledge of the inner anatomical structures of the neck. The neck would be simplified into a mechanical model, and utilizing the magnitude of the external force at the determined angle, the reaction forces on the neck joint could be calculated.

Chapter 4: Conclusion

In conclusion, this research was successful in the development of a micro-scale motion capture system to track markers on the head, thorax, and abdomen of an ant. The system was able to produce results with relatively low error, in addition to the ability to track the 3D angle between the head, abdomen, and thorax markers during movement. The ability to determine the range of motion of the ant brings us one step closer to accurately derive biomechanical data from the internal neck structure.

Several limitations were encountered during this research, with the main issue being the inability to control the movement of the ants during filming. The brood was the only source of incentive provided to motivate the ants to lift and carry an external load; however, the ants appeared more concerned by their new surroundings than the brood. The majority of the time, the ants' activity centered on trying to escape by climbing up the walls of the testing environment. Hours of film were recorded in order to produce seconds of trackable footage. In addition, even though the overall procedure produced accurate results, the video processing was heavily user involved and time consuming. Another large limitation was the use of only one camera from the side view. In an ideal set-up, there would be 4 orthogonal cameras on the sides of the environment, with one camera mounted on the top. A future recommendation would be to redesign the environment to allow for more cameras to be utilized and to find an object the ants are willing to lift and carry.

Research related to the study of the ant neck will be continued by graduate student Ryan Wilbur, whose focus is to create highly detailed models of the neck through Micro-CT scans. The

discovery of the internal structures of the neck will allow the development of anthropometric data of the carpenter ants, which will aid in biomechanical analysis.

References

[1] Wojtusiak, J., E.J. Godzinska, and A. Dejean. “Capture and Retrieval of Very Large Prey by Workers of the African Weaver Ant.” *Tropical Zoology*, vol. 8, no. 2, pp. 309-318, 1995.

[2] Castro, C., Katsube, N., and Lilly, B. “Reverse Engineering the Functional Design of the Ant Neck Joint.” *IOS Preliminary Proposal*, 2013.

[3] Nguyen, V., Lilly, B., and Castro, C. “The Exoskeletal Structure and Tensile Loading Behavior of an Ant Neck joint.” *The Journal of Experimental Biology,* 2012.

[4] Tsuda, Hiromi. “Analysis of Ant Neck Tissue Using Scanning Electron Microscopy Imaging (SEM).” *The Ohio State University*, 2015.

[5] Kakumani, Akul. “Design of a Tensile Tester to Test an Ant Neck Joint.” *The Ohio State University*, 2017.

[6] Moeslund, Thomas B., Adrian Hilton, and Volker Krüger. "A survey of advances in vision-based human motion capture and analysis." *Computer vision and image understanding* 104.2-3 (2006): 90-98.

[7] Winter, David A. *Biomechanics and Motor Control of Human Movement*. J. Wiley, pp. 86-89, 2005.

[8] Gibson, D. P., et al. “Capture and Synthesis of Insect Motion.” *Proceedings of the 2005 ACM SIGGRAPH/Eurographics Symposium on Computer Animation - SCA '05*, 2005, doi:10.1145/1073368.1073374.

[9] Bender, John A., et al. “Computer-Assisted 3D Kinematic Analysis of All Leg Joints in Walking Insects.” *PLoS ONE*, vol. 5, no. 10, 2010, doi:10.1371/journal.pone.0013617.

[10] “PolarPro Macro Lens for GoPro Hero4 - 3.8X Magnification Filter : Camera & Photo.”*Amazon.com : PolarPro Macro Lens for GoPro Hero4 - 3.8X Magnification Filter : Camera & Photo*, www.amazon.com/PolarPro-Macro-Lens-GoPro-Hero4/dp/B00GV8QO2I/ref=sr_1_1/161-9672321-0068253?ie=UTF8&qid=1484327292&sr=8-1&keywords=go%2Bpro%2Bhero%2B4%2Bmacro%2Blens.

[11] “Neewer 12.5X Magnification Macro Close up Lens with Adapter Ring for Gopro Hero 3 3+ 4, Fit Gopro Hero Body Without Any Diving House : Camera & Photo.” Amazon.com : Neewer 12.5X Magnification Macro Close up Lens with Adapter Ring for Gopro Hero 3 3+ 4, Fit Gopro Hero Body Without Any Diving House: Camera & Photo, www.amazon.com/Neewer-Magnification-Adapter-Without-Diving/dp/B01EWK42SO/ref=sr_1_3/161-9672321-0068253?ie=UTF8&qid=1484327292&sr=8-3&keywords=go%2Bpro%2Bhero%2B4%2Bmacro%2Blens.

[12] Hölldobler, Bert, and Edward O. Wilson. *Journey to the Ants: a Story of Scientific Exploration*. Belknap Press, pp. 219, 1995.

[13] Marlow, Michael. “Black and White, Ant or Less.” *BugPhoto.net*, 3 July 2014, bugphoto.net/2013/11/21/black-and-white-ant-or-less/. (figure 11)

[14] Wunderlich, Bruce. “Understanding Depth of Field for Beginners.” *Digital Photography School*, 9 Nov. 2017, digital-photography-school.com/understanding-depth-field-beginners/.

[15] Black, Dave, et al. “Understanding Focal Length.” *Focal Length | Understanding Camera Zoom & Lens Focal Length | Nikon from Nikon*, www.nikonusa.com/en/learn-and-explore/a/tips-and-techniques/understanding-focal-length.html.

[16] Zorlu, Mustafa. “ANT.” *GrabCAD - CAD Library*, 4 Jan. 2013, grabcad.com/library/ant--2.

[17] Myers, Tom. “Pest World For Kids.” *Ants - Facts About Ants - Types of Ants - PestWorldforKids.org*, pestworldforkids.org/pest-guide/ants/.

[18] Go Pro Site: “Search.” *GoPro Official Website*- Capture + Share Your World- Homepage, gopro.com/help/search.

Appendix

Position Vs. Time & Error Graphs for Ants 1:5

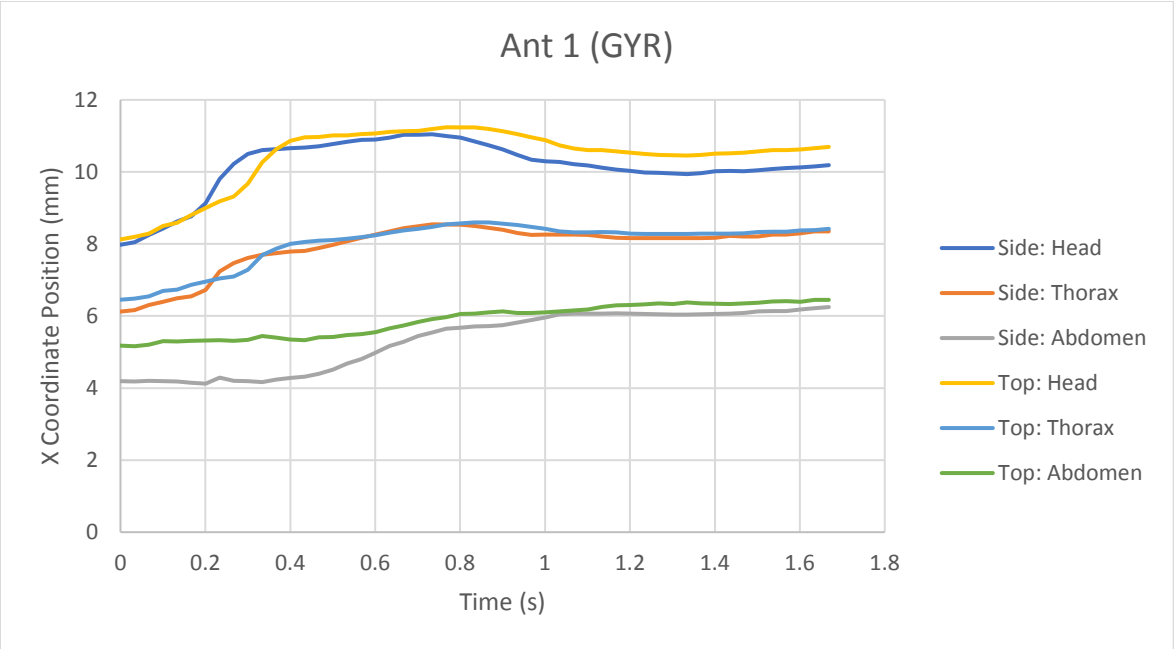

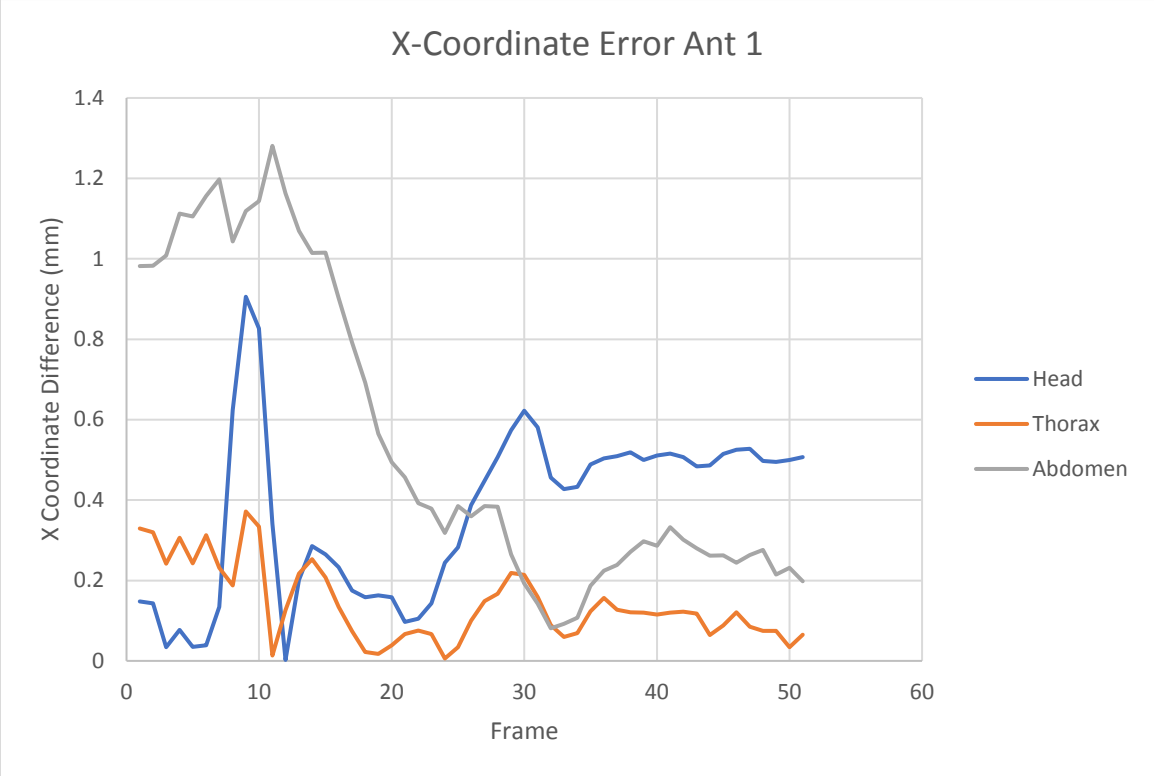

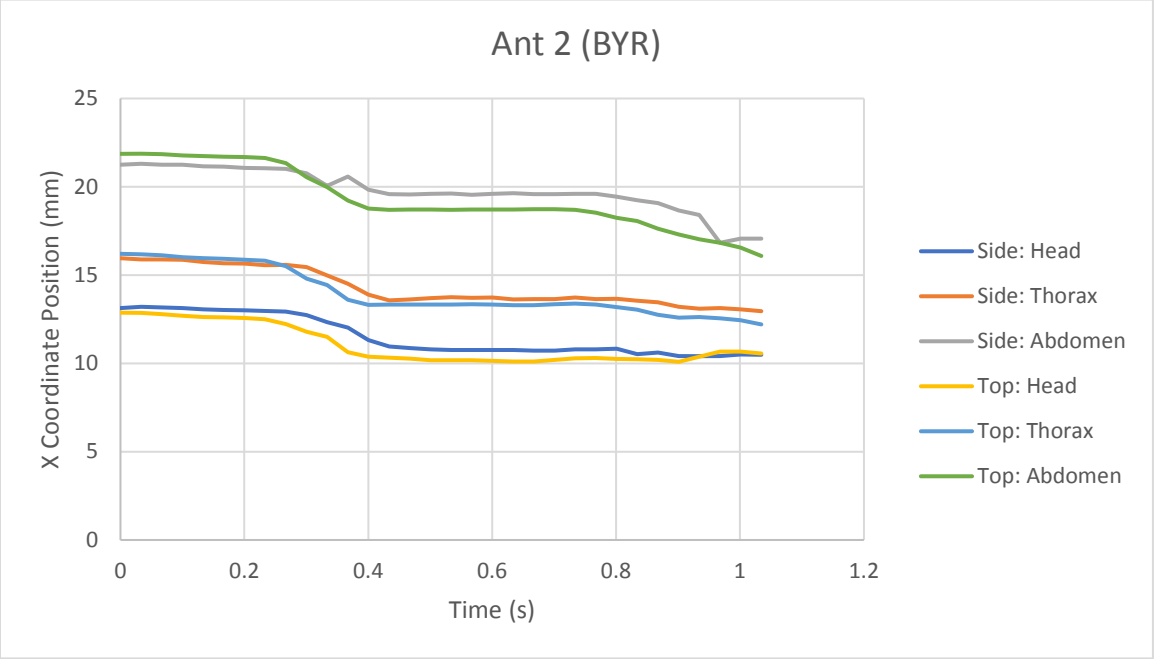
Ant 2 (BYR)
X Coordinate Position (mm)
25
20
15
10
5
0
0
0.2
0.4
0.6
0.8
1
1.2
Time (s)
Side: Head
Side: Thorax
Side: Abdomen
Top: Head
Top: Thorax
Top: Abdomen

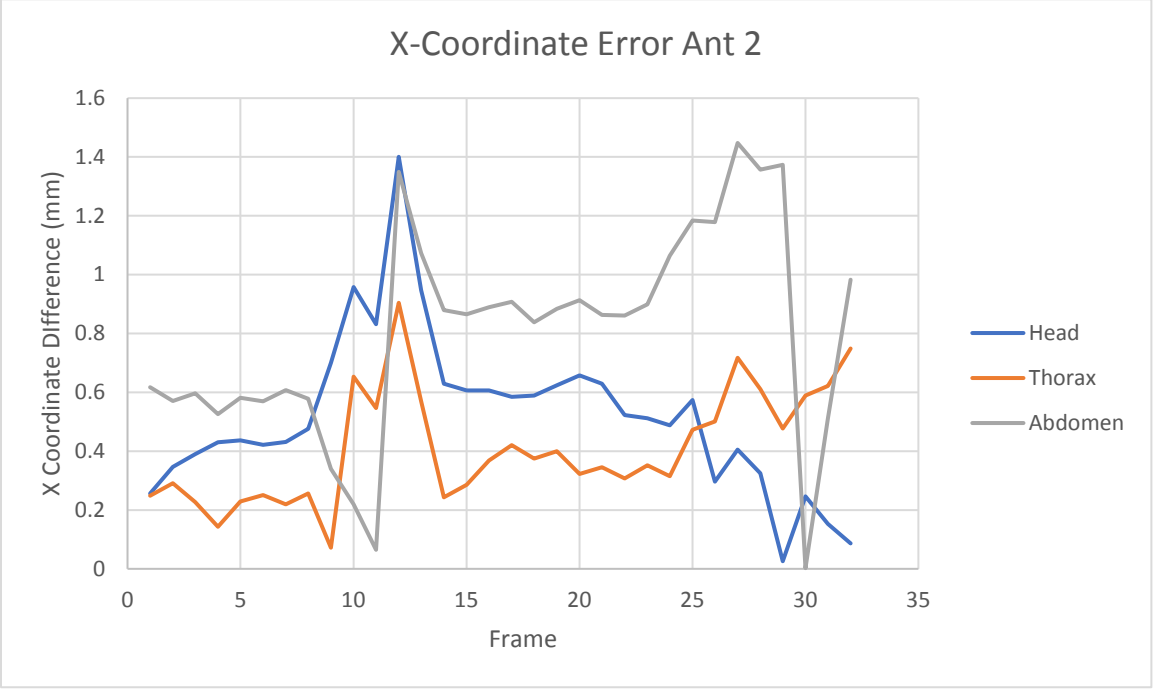
X-Coordinate Error Ant 2
X Coordinate Difference (mm)
1.6
1.4
1.2
1
0.8
0.6
0.4
0.2
0
0
5
10
15
20
25
30
35
Frame
Head
Thorax
Abdomen

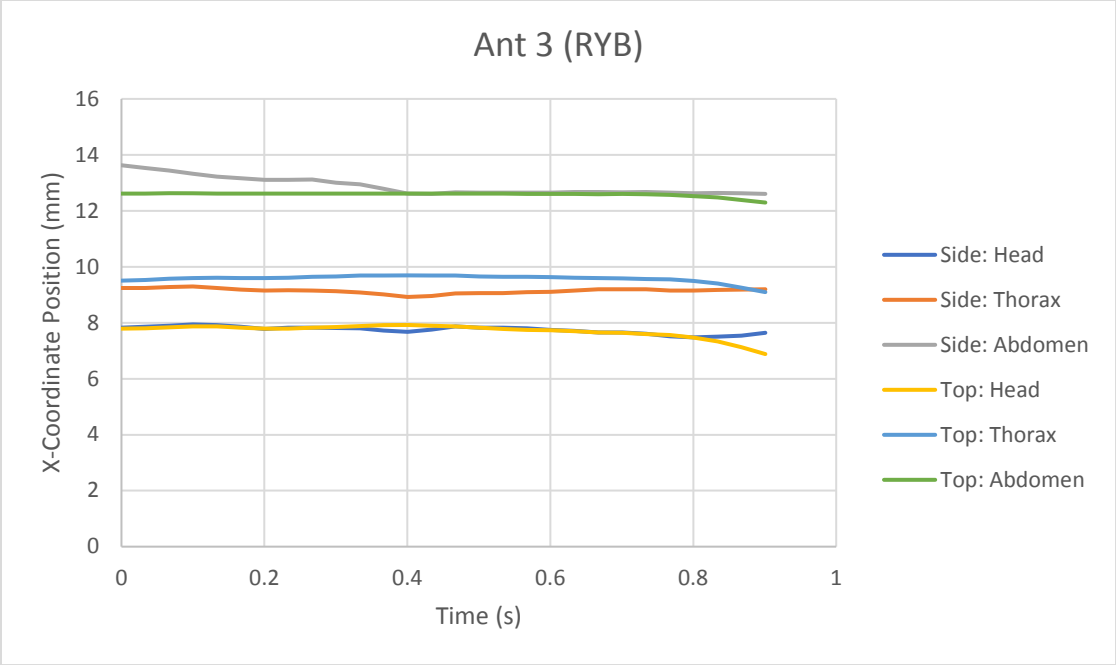
Ant 3 (RYB)
X-Coordinate Position (mm)
16
14
12
10
8
6
4
2
0
0
0.2
0.4
0.6
0.8
1
Time (s)
Side: Head
Side: Thorax
Side: Abdomen
Top: Head
Top: Thorax
Top: Abdomen

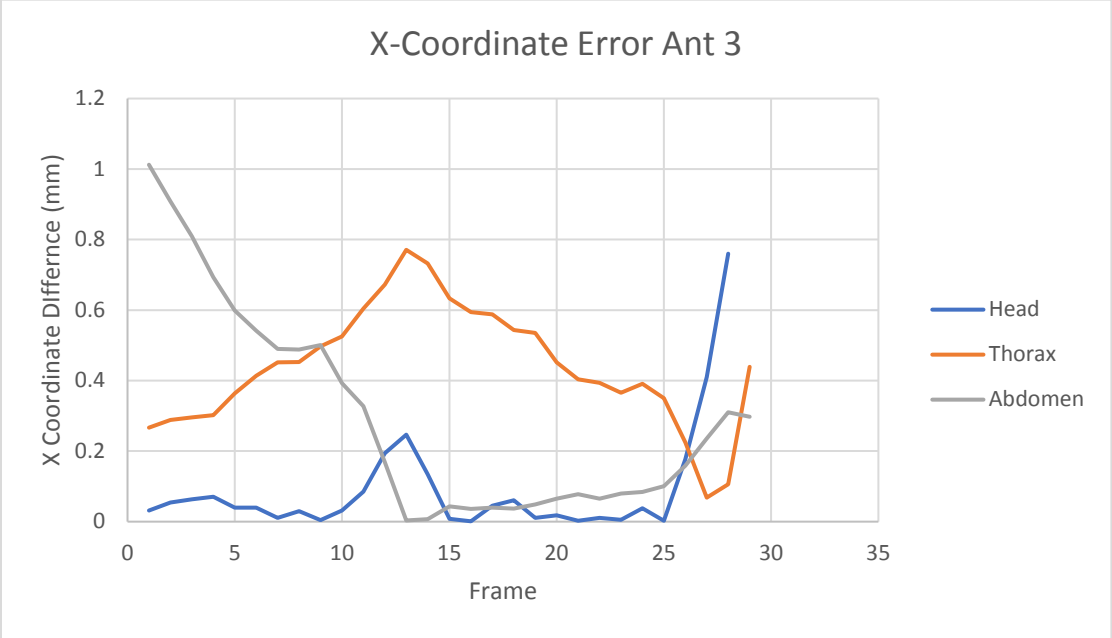
X-Coordinate Error Ant 3
X Coordinate Differnce (mm)
1.2
1
0.8
0.6
0.4
0.2
0
0
5
10
15
20
25
30
35
Frame
Head
Thorax
Abdomen

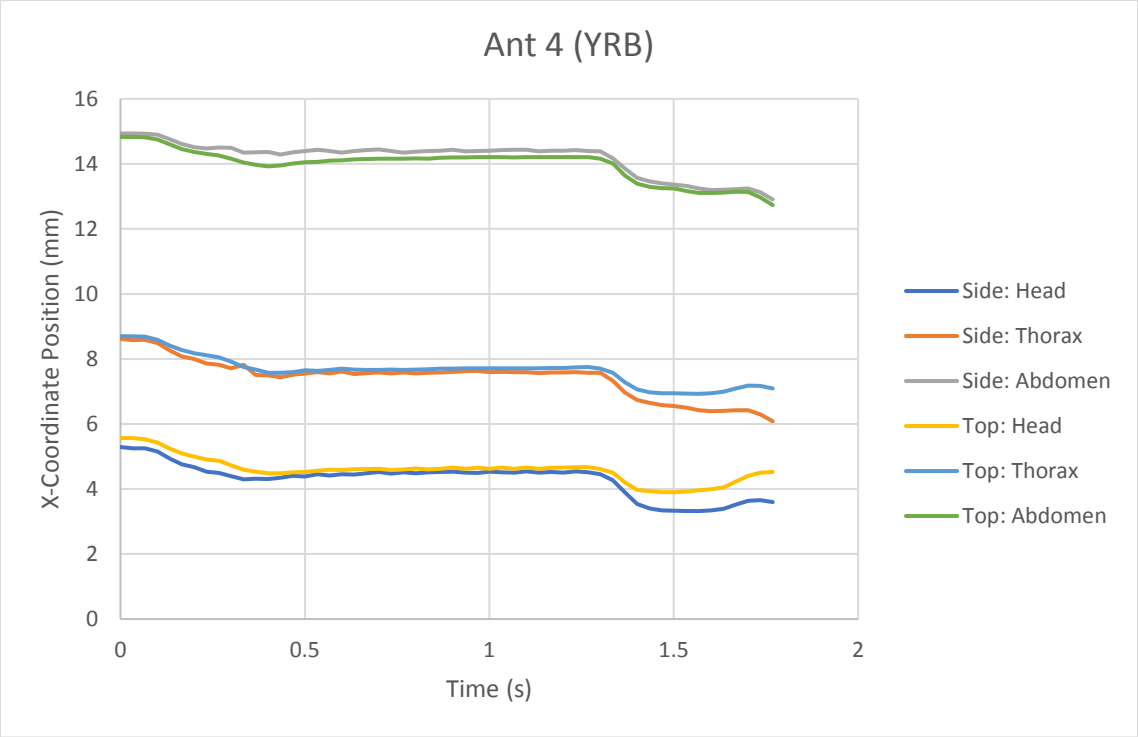
Ant 4 (YRB)
X-Coordinate Position (mm)
16
14
12
10
8
6
4
2
0
0
0.5
1
1.5
2
Time (s)
Side: Head
Side: Thorax
Side: Abdomen
Top: Head
Top: Thorax
Top: Abdomen

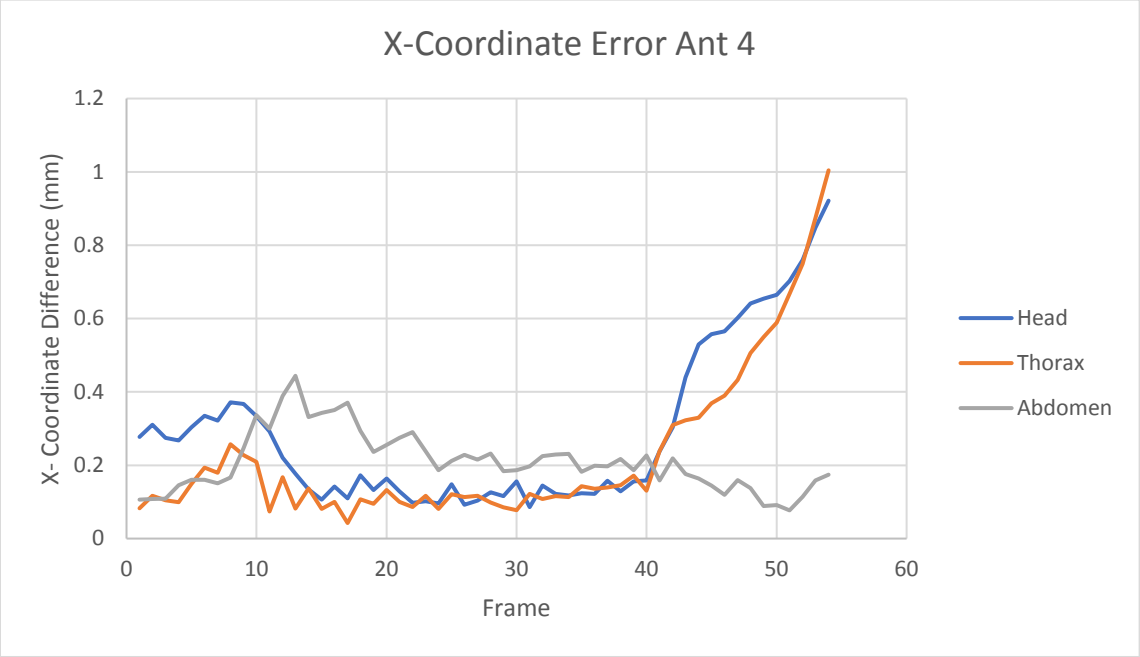
X-Coordinate Error Ant 4
X- Coordinate Difference (mm)
1.2
1
0.8
0.6
0.4
0.2
0
0
10
20
30
40
50
60
Frame
Head
Thorax
Abdomen

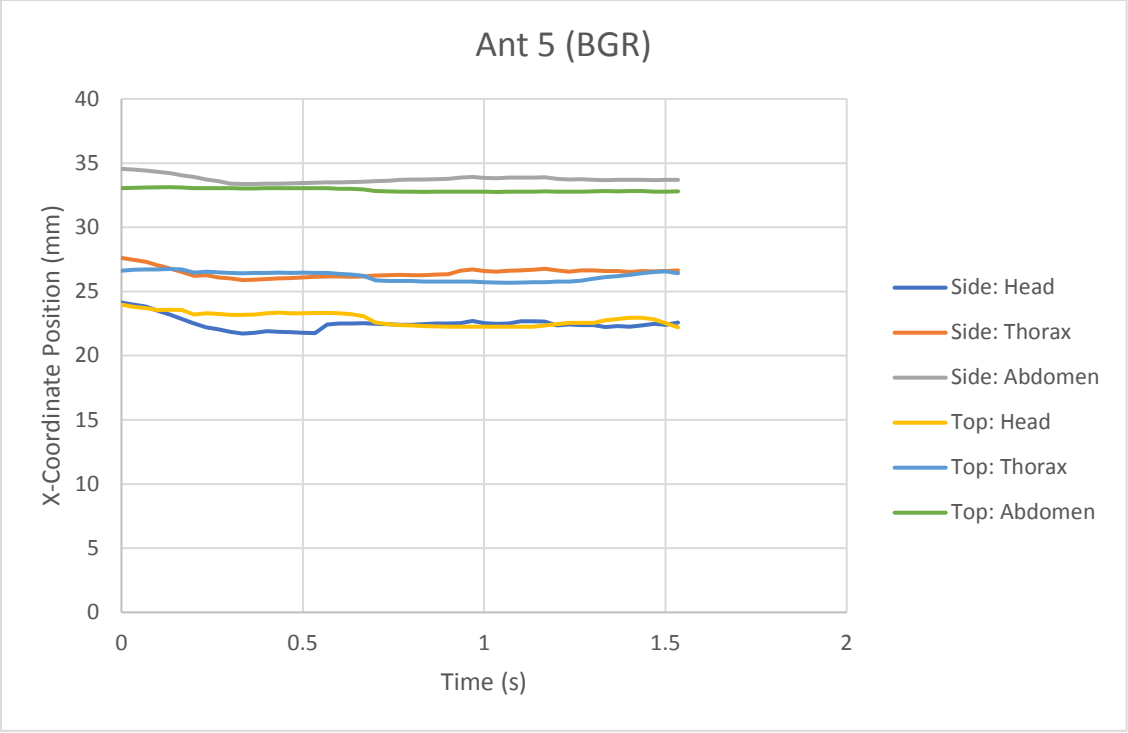
Ant 5 (BGR)
X-Coordinate Position (mm)
Time (s)
Side: Head
Side: Thorax
Side: Abdomen
Top: Head
Top: Thorax
Top: Abdomen

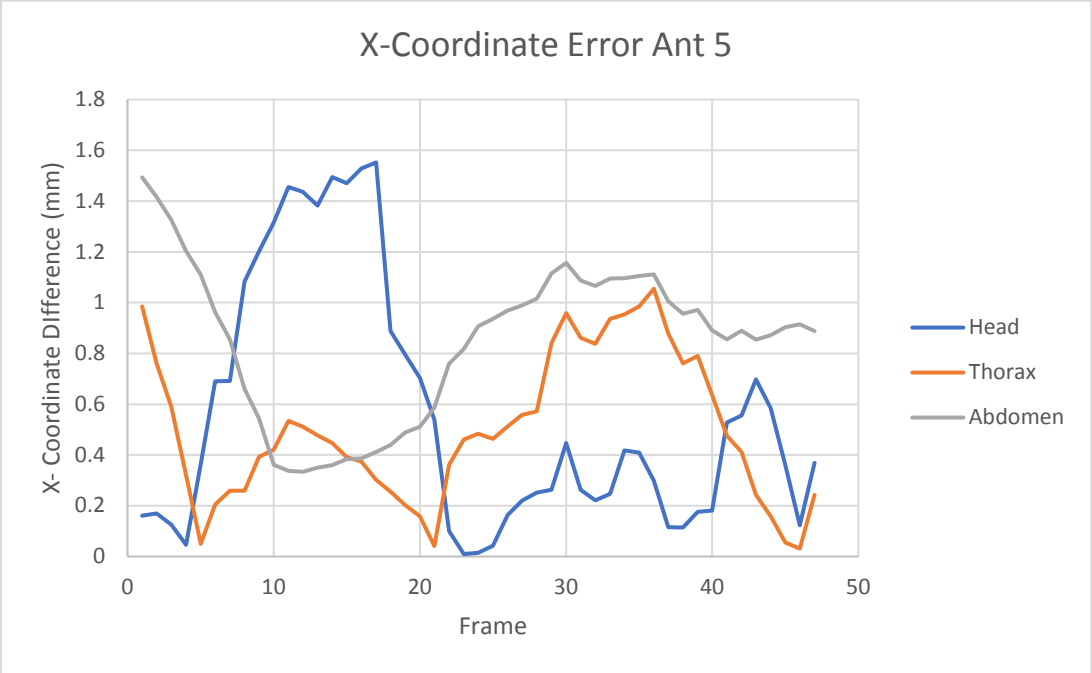
X-Coordinate Error Ant 5
X- Coordinate Difference (mm)
Frame
Head
Thorax
Abdomen

Graphs of Projected angles & 3D angle vs. time from Matlab

Ant 0

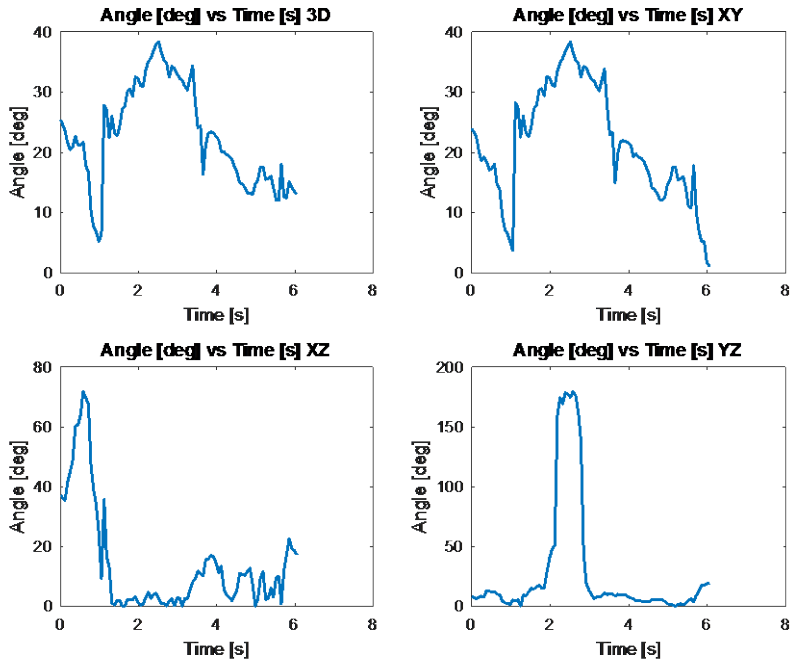

Ant 1

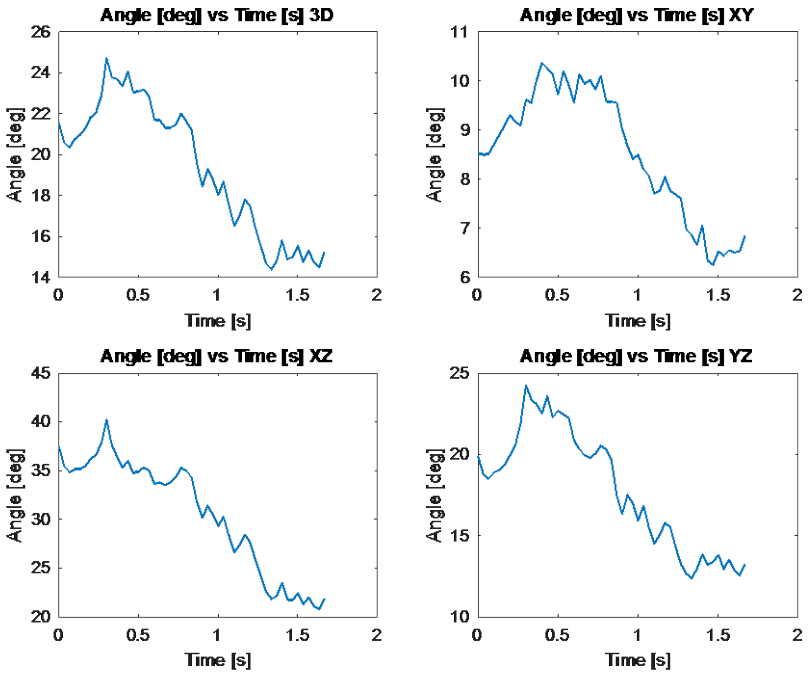

Ant 2

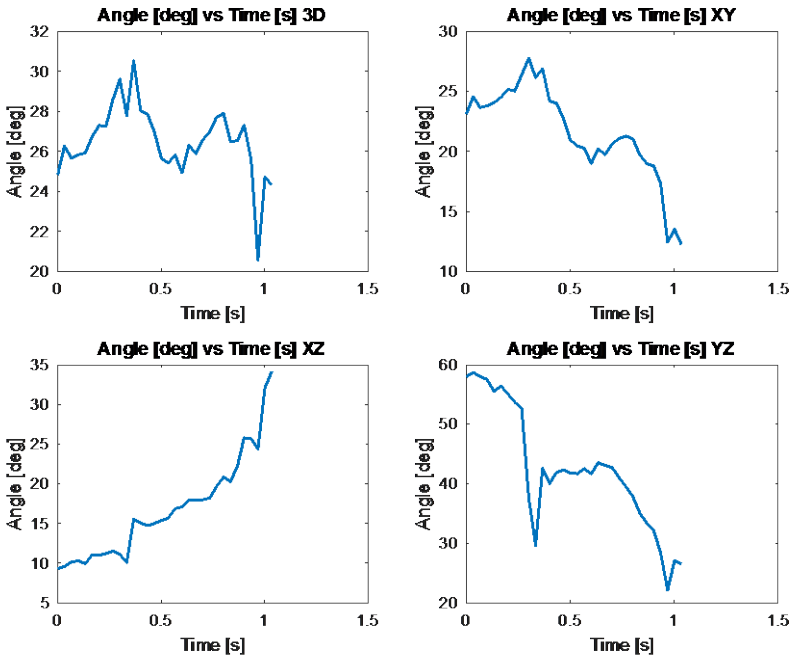
Angle [deg] vs Time [s] 3D
Angle [deg]
Time [s]
Angle [deg] vs Time [s] XY
Angle [deg]
Time [s]
Angle [deg] vs Time [s] XZ
Angle [deg]
Time [s]
Angle [deg] vs Time [s] YZ
Angle [deg]
Time [s]

Ant 3

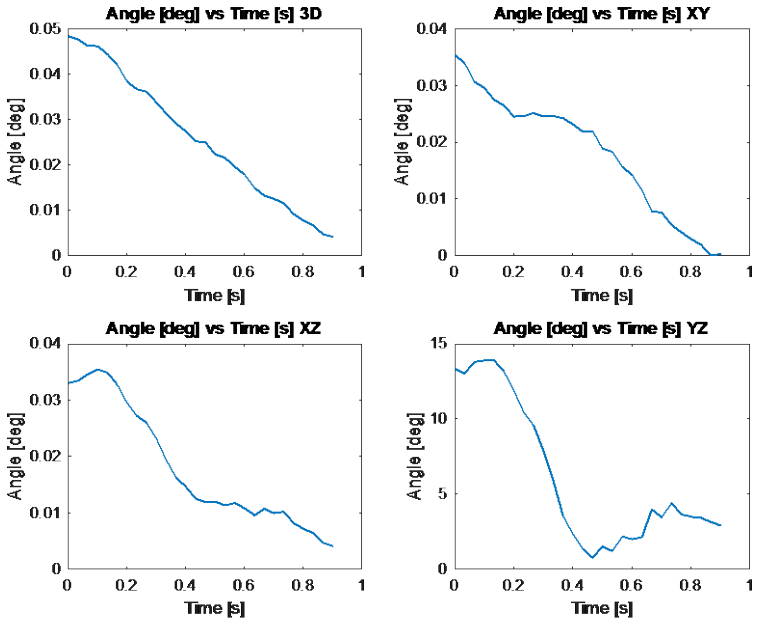
Angle [deg] vs Time [s] 3D
Angle [deg]
Time [s]
Angle [deg] vs Time [s] XY
Angle [deg]
Time [s]
Angle [deg] vs Time [s] XZ
Angle [deg]
Time [s]
Angle [deg] vs Time [s] YZ
Angle [deg]
Time [s]

Ant 4

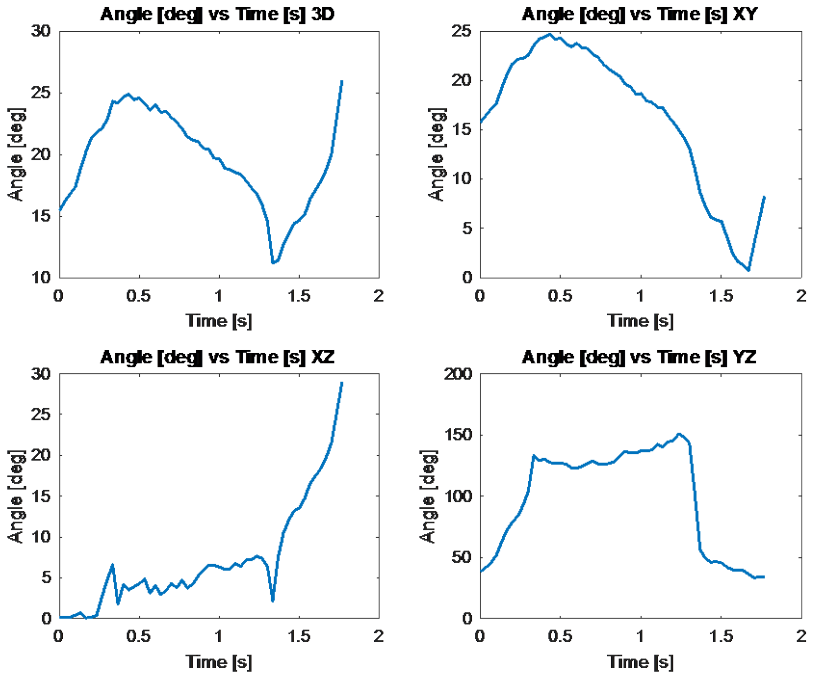
Angle [deg] vs Time [s] 3D
Angle [deg]
Time [s]
Angle [deg] vs Time [s] XY
Angle [deg]
Time [s]
Angle [deg] vs Time [s] XZ
Angle [deg]
Time [s]
Angle [deg] vs Time [s] YZ
Angle [deg]
Time [s]

Ant 5

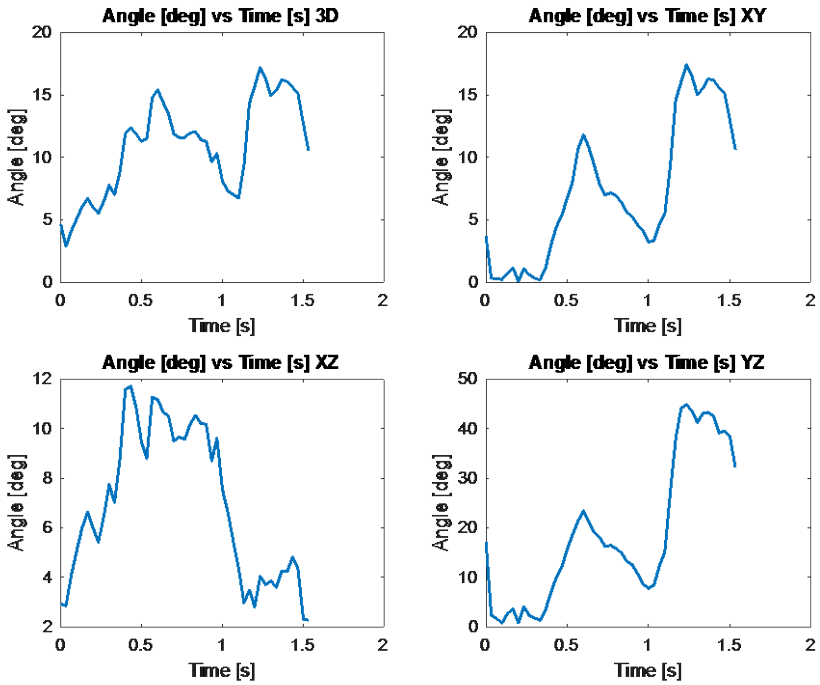
Angle [deg] vs Time [s] 3D
Angle [deg]
Time [s]
Angle [deg] vs Time [s] XY
Angle [deg]
Time [s]
Angle [deg] vs Time [s] XZ
Angle [deg]
Time [s]
Angle [deg] vs Time [s] YZ
Angle [deg]
Time [s]

Matlab Code for Calculating Angles

Script:

```
clc
clear all
close all

%% Import Excel Data
S = importdata('antData_2.xlsx');
sheets = S.data;
allSheets = {sheets.Ant0_WWW sheets.Ant1_GYR sheets.Ant2_BYR sheets.Ant3B_RYB sheets.Ant4_YRB sheets.Ant5_BGR};

for k = 1:length(allSheets)

    antData = allSheets{k};
    [m,n] = size(antData);

    %% Intialize Arrays
    vec1 = cell(m,3);
    vec2 = cell(m,3);

    vec1XY = cell(m,2);
    vec2XY = cell(m,2);

    vec1XZ = cell(m,2);
    vec2XZ = cell(m,2);

    vec1YZ = cell(m,2);
    vec2YZ = cell(m,2);

    ANG = zeros(m,1);
    XY = zeros(m,1);
    XZ = zeros(m,1);
    YZ = zeros(m,1);

    %% Populate Arrays (x,y,z for each marker)
    time = antData(1:end,1);

    xAS = antData(1:end,2);
    zAS = antData(1:end,3);

    xBS = antData(1:end,5);
    zBS = antData(1:end,6);

    xCS = antData(1:end,8);
    zCS = antData(1:end,9);

    xAT = antData(1:end,11);
    yAT = antData(1:end,12);

    xBT = antData(1:end,14);
    yBT = antData(1:end,15);

    xCT = antData(1:end,17);
    yCT = antData(1:end,18);

    xA_avg = (xAS + xAT)/2;
    xB_avg = (xBS + xBT)/2;
    xC_avg = (xCS + xCT)/2;

    A = {xA_avg, yAT, zAS};
    B = {xB_avg, yBT, zBS};
    C = {xC_avg, yCT, zCS};

    %% Create vector from marker A -> B
    AB = {A{1}-B{1}, A{2}-B{2}, A{3}-B{3}};

    %% Create vector from marker B -> C
    BC = {B{1}-C{1}, B{2}-C{2}, B{3}-C{3}};

    for i = 1:length(xAS)
        vec1{i} = [AB{1}(i), AB{2}(i), AB{3}(i)];
```

```
        vec2{i} = [BC{1}(i), BC{2}(i), BC{3}(i)];

        vec1XY{i} = [AB{1}(i), AB{2}(i)];
        vec2XY{i} = [BC{1}(i), BC{2}(i)];

        vec1XZ{i} = [AB{1}(i), AB{3}(i)];
        vec2XZ{i} = [BC{1}(i), BC{3}(i)];

        vec1YZ{i} = [AB{2}(i), AB{3}(i)];
        vec2YZ{i} = [BC{2}(i), BC{3}(i)];

        %% Dot product to obtain angle between three points in all planes
        ANG(i) = acosd(dot(vec1{i},vec2{i})/(norm(vec1{i})*norm(vec2{i})));

        XY(i) = acosd(dot(vec1XY{i},vec2XY{i})/(norm(vec1XY{i})*norm(vec2XY{i})));
        XZ(i) = acosd(dot(vec1XZ{i},vec2XZ{i})/(norm(vec1XZ{i})*norm(vec2XZ{i})));
        YZ(i) = acosd(dot(vec1YZ{i},vec2YZ{i})/(norm(vec1YZ{i})*norm(vec2YZ{i})));
    end

    fig = figure(k);
    subplot(2,2,1);
    plot(time,ANG,'Linewidth',1.5);
    xlabel('Time [s]');
    ylabel('Angle [deg]');
    title('Angle [deg] vs Time [s] 3D');
    grid on

    subplot(2,2,2);
    plot(time,XY,'Linewidth',1.5);
    xlabel('Time [s]');
    ylabel('Angle [deg]');
    title('Angle [deg] vs Time [s] XY');
    grid on

    subplot(2,2,3);
    plot(time,XZ,'Linewidth',1.5);
    xlabel('Time [s]');
    ylabel('Angle [deg]');
    title('Angle [deg] vs Time [s] XZ');
    grid on

    subplot(2,2,4);
    plot(time,YZ,'Linewidth',1.5);
    xlabel('Time [s]');
    ylabel('Angle [deg]');
    title('Angle [deg] vs Time [s] YZ');
    grid on

    saveas(fig,strcat('ant_',num2str(k-1),'.jpg'));

    disp('Ant:')
    disp(k-1)
    disp('Max Angle:')
    disp(max(ANG));
    disp('Min Angle:')
    disp(min(ANG));
    disp('Delta Angle:')
    disp(max(ANG) - min(ANG));

end
```

Command:

```
Ant:
     0

Max Angle:
   38.3667

Min Angle:
```

5.3147

Delta Angle:
33.0520

Ant:
1

Max Angle:
24.7051

Min Angle:
14.4061

Delta Angle:
10.2991

Ant:
2

Max Angle:
30.5465

Min Angle:
20.5691

Delta Angle:
9.9774

Ant:
3

Max Angle:
0.0484

Min Angle:
0.0041

Delta Angle:
0.0443

Ant:
4

Max Angle:
26.0079

Min Angle:
11.2067

Delta Angle:
14.8012

Ant:
5

```
Max Angle:
   17.2004

Min Angle:
    2.8737

Delta Angle:
   14.3266

>>
```